Development of a Novel Exergy Tool for Realizing an Energy Efficient Naphtha Reforming Process

Name: Jawad Mustafa

Reg No: 00000117226

This work is submitted as a MS thesis in partial fulfillment of the requirement for the degree of MS in Chemicals Engineering

Supervisor Name: Dr. Iftikhar Ahmad

School of Chemical and Materials Engineering (SCME)

National University of Sciences and Technology (NUST),

H-12 Islamabad, Pakistan

September, 2017

Abstract

In order to realize an energy-efficient naphtha reforming process, various energy analysis methods are adopted. These methods are based on the first law of thermodynamics or a combination of the first and second law of thermodynamics. The conventional method of energy analysis based on the first law of thermodynamics is inadequate because it cannot grasp the effect of system irreversibilities. Exergy analysis which embeds second law of thermodynamics in the conventional method overcomes this deficiency and represents the true thermodynamic efficiency of the process. In this work, a novel technique based on computational fluid dynamics is proposed to perform exergy analysis of naphtha reforming reactors. N-heptane cut of naphtha reforming process which comprises of paraffin, aromatics and naphthene are used to conduct this analysis. Three reactors, connected in series, are used and all the three types of exergy, i.e., physical exergy, chemical exergy and mixing exergy, are examined. It is analyzed that the physical and mixing exergy in the reactors is decreasing along the length of the reactors whereas the chemical energy increases due to the high chemical potential of products.

Acknowledgement

First and foremost, praises and thanks to ALLAH, the Almighty, for His showers of blessings throughout my research work to complete the research successfully.

This dissertation would not have been possible without the guidance and the help of several individuals who in one way or another contributed and extended their valuable assistance in the preparation and completion of this study.

Firstly, my profound gratitude and deep regards to my research supervisor, **Dr. Iftikhar Ahmad Salarzai** for his endless support, supervision and affectionate guidance. His exemplary guidance, steadfast encouragement, perceptive criticism and valuable suggestions were of immense help throughout my project work and shall carry me a long way in the journey of life on which I am about to embark.

I am deeply obliged to **Dr. Muhammad Ahsan** and **Dr. Tayyaba Noor** for their kind co-operation throughout the course of this project.

I would like to extend my heartfelt thanks to **Dr. Arshad Hussain** (Principal, School of Chemical and Materials Engineering) for providing a research oriented platform to effectively utilize my skills in accomplishing this research work.

Last but not the least, I am extremely grateful to my parents for their love and prayers for educating and preparing me for future. This accomplishment would not have been possible without them.

Jawad Mustafa

Nomenclature

E	Total molar exergy
E^{ph}, E^{ch}, $E^{\Delta mix}$	Molar physical, chemical and mixing exergy
C_{Pi}^{mean}	Mean heat capacity of i component
X	Mole fraction
L_0 , V_0	liquid and vapor fraction of the stream at a reference temperature and pressure
e_i	Standard chemical exergy
$\Delta_f G_i^0$	Standard Gibbs free energy of formation of component
T_0 , P_0	Reference temperature and pressure
H , S	Molar enthalpy and entropy at reference temperature and pressure
E_{in}	Exergy of feed at the inlet of reactor
E_{out}	Exergy at the outlet of the reactor
n_i	No of moles of component i
P_i	Static pressure of component i
z	No of components
η	Exergetic efficiency

Contents

List of Figures

List of Tables

Chapter-1

Introduction

1.1 Background

Uninterrupted supply of energy is inevitable for modern age developments and technological advancements. Fossils fuels are major contributor in today's energy resources. However, these fuels will be exhausted and are contributing in global climate change due to tremendous amount of greenhouse gas emissions. Other energy resources have same inherent issues at few or all stages of energy generation. Figure 1.1 and figure 1.2 shows worlds fuel consumption by source and CO_2 emissions.

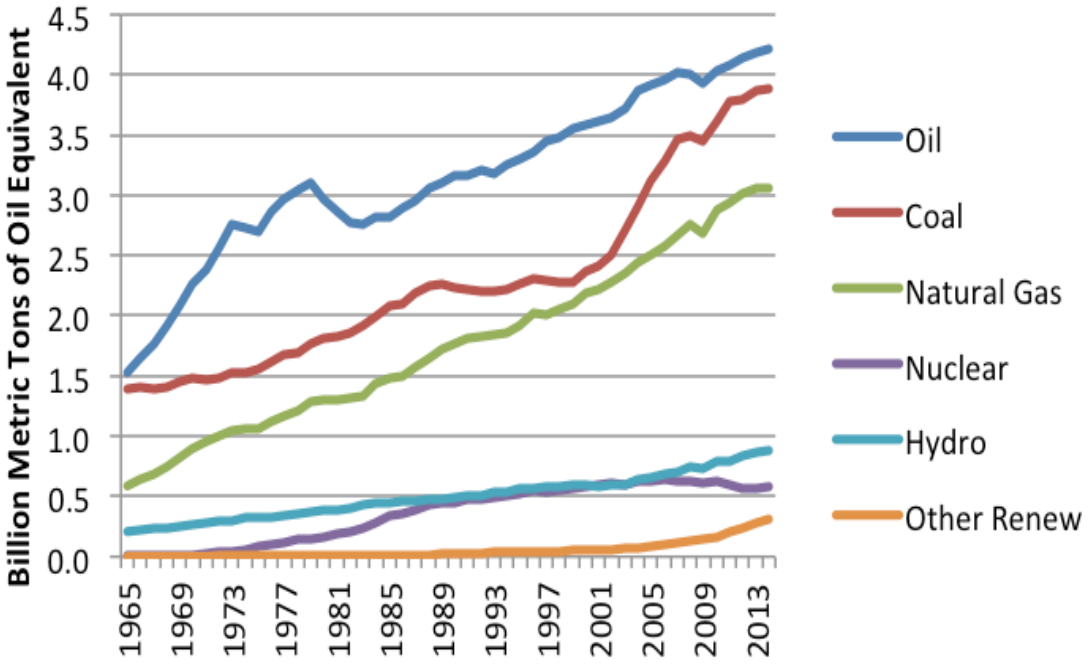

Figure 1.1: World's fuel consumption by source [1]

Energy is the lifeline of this modern world and chemical industry is its backbone. Three basic outputs of a chemical industry, i.e. basic chemicals, specialty chemicals and consumer chemicals, covers a wide range of products in sectors ranging from electronics, energy, transportation, telecommunications, pharmaceuticals to buildings. Being a biggest manufacturing sector and due to the energy intensive chemical manufacturing processes,

in 2013 chemical industry contributes roughly 10% towards global energy consumption and about 7% towards greenhouse gas emissions (GHQ) made by global industry. This consumption is expected to increase by 40% in 2040 as shown in figure 1.3

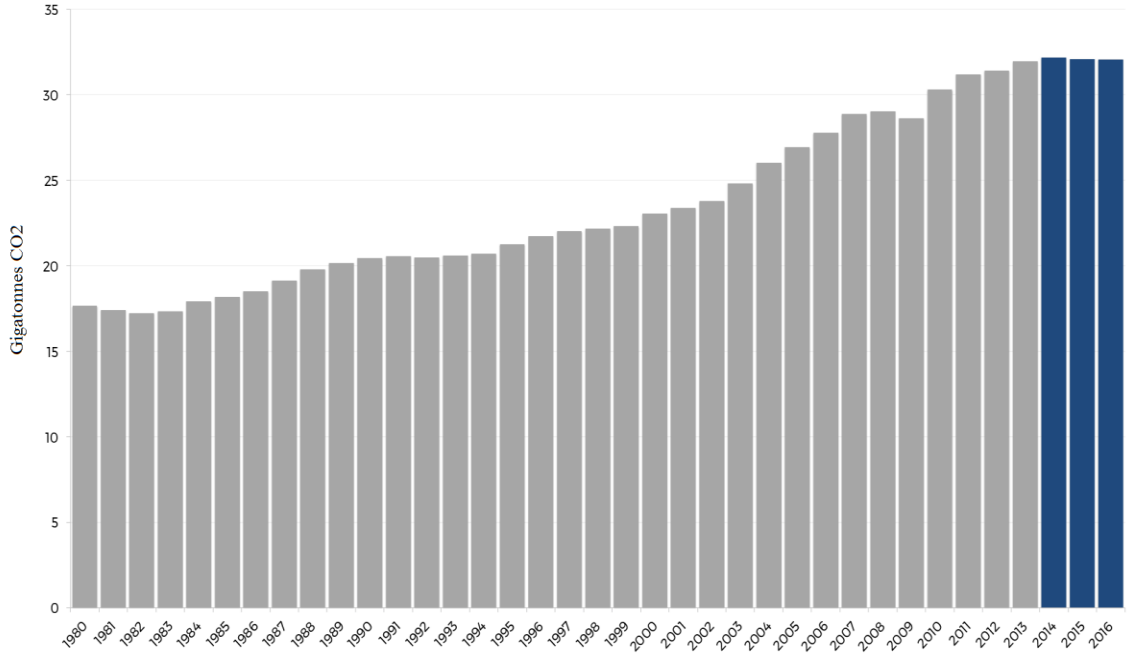

Figure 1.2: World's CO_2 emission [2]

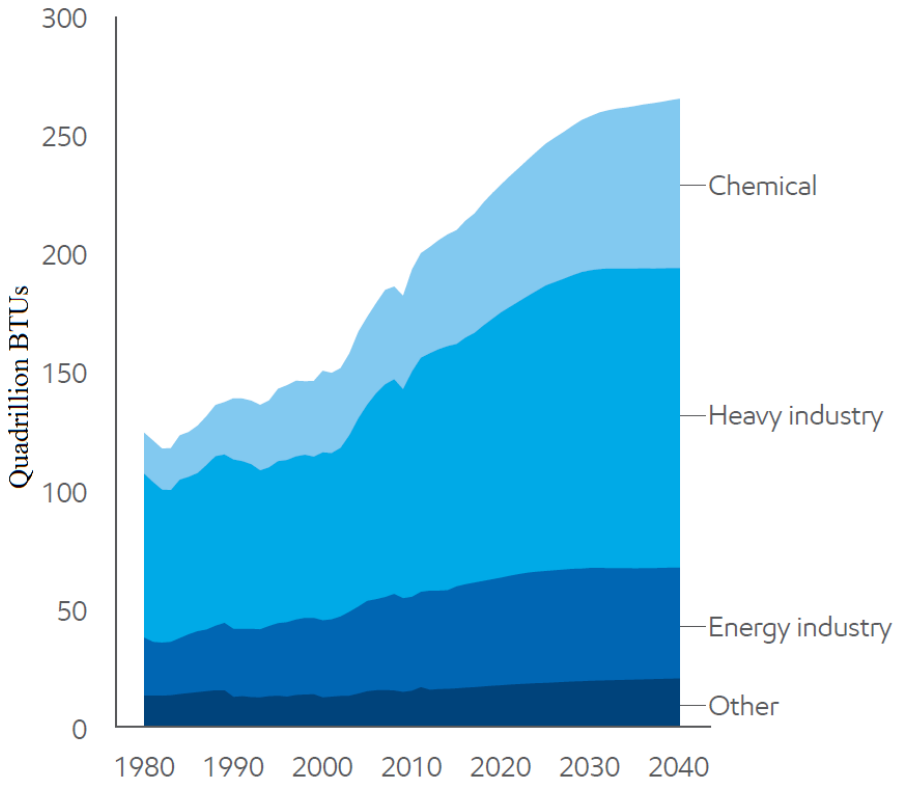

Figure 1.3: Forecast of industrial energy demand by 2040 [1]

Improvements in catalyst technologies and implementation of best practice technologies have enabled chemical process industries to lower its energy consumption and curtail its greenhouse gas emissions. But still there is a lot of room for improvement and a further need to improve the energy efficiencies of chemical processes. One promising method to achieve it is an exergy analysis. Current energy analysis techniques only quantify the energy being wasted compared to energy inputs, regardless of the quality of the energy and its potential to drive a real process. Thus, energy efficiency only involves conserving as much energy as possible relative to energy inputs. On the other hand, exergy quantifies the work being wasted relative to energy/work inputs and exergetic efficiencies focuses on (destroying and wasting as little work as possible,) providing a better potential for improvement.

During an energy conversion process, there is a loss in quality of energy, thus to extract as much exergy as possible from an energy conversion process should be a real goal. In a chemical process, heat loss is relatively easy to locate and hence a lot of attention and

resources are employed to prevent it. However, work loss or irreversibilities arising in a chemical process are not often identifiable and a deeper analysis is required to expose them. So, they are often ignored, regardless of the fact that there is an economic cost related to them. Exergy analysis is a potential method that can identify and quantify these irreversibilities and work loss associated with them. This providing a room for improvement and potential for cost savings.

There is still a very little adoption of exergy analysis in chemical industries and chemical process designing. This is due to lack of knowledge, training and standardize tool for exergy analysis in the industrial sector. The motivation of this research is to develop a computational model that can easily be utilized during designing or operational stage of most chemical manufacturing processes. This tool should be flexible enough to be tamed as required, but also be rigorous enough to cope with complex calculations needed for exergy analysis.

1.2 Thesis Outline

Chapter 1 portrays the background and motivation of the research work. Basic theoretical concepts governing exergy and naphtha reforming process are described in chapter 2. In chapter 3, procedure for CFD based model development is discussed. In chapter 4, literature survey is depicted about the latest development to evaluate the exergy. Chapter 5 illustrates the development of exergy quantification tool. In this chapter details of geometry preparation and simulation are discussed in this chapter. Results, conclusions and future recommendations are described in Chapter 6 and 7 respectively.

Chapter-2

Theoretical Background

2.1 Components of Energy

Any form of energy can be subdivided in two main components, one which can produce work while the other which cannot be used in any real process to generate work. Later one is called anergy while the former one is termed as exergy. Thus a form of energy with greater exergy component is of higher quality than the one having more anergy associated with it. The idea of maximum available work is not new and has been continuously developed by many researchers in 19^{th} and 20^{th} under a different description. However, the term exergy itself was first introduced by Zoran Rant in 1956 by combining two Greek words ex and ergon meaning "from work". Table 2.1 describes exergy and some of the related concepts. Exergy can be defined as;

> "The maximum possible work obtainable by bringing a matter from its initial state through a reversible process to a state of unrestricted thermodynamic and chemical equilibrium with the reference environment, referred as dead state [3]".

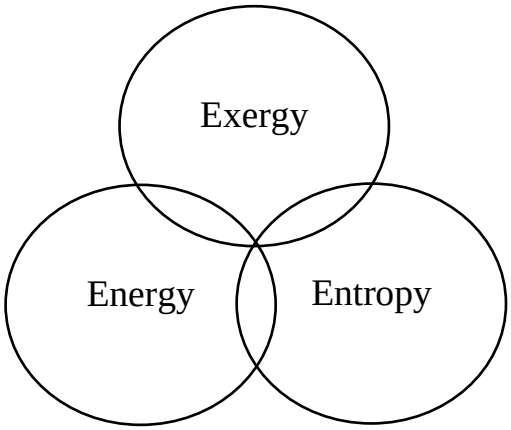

Figure 2.1: Interaction of energy, entropy and exergy

Exergy can be utilized as a standard to define quality of energy as it is the only component actually producing work. Exergy is related to ideal work as entropy generation has a direct link with exergy through second law of thermodynamics. Rate of entropy generation is directly proportional to exergy loss which leads to degradation of exergy in a real process. Thus, the goal of any energy transformation process should be to extract highest possible exergy out of energy input, as more exergy translates into more work.

Table 2.1: Related concepts of Exergy [4]

Year	Author	Designation
1824	Carnot	Pauissance Motrice du feu
1872	Thomson	Motivity
1873	Gibbs	Available energy of the body and medium
1881	Gouy	Energie utilizable
1898	Stodola	Freie techische energie
1925	Debaufre	Available energy
1935	Bonjakovic	Technische arbeitsfahigkeit
1944	Thring	Virtue of energy
1953	Schmidt	Technische maximale arbeit
1955	Gibert	Energie non degrade
1956	Grigull	ekthalpie

2.2 Reference Environment

A main advantage of the thermodynamic concept of exergy is that calculations of exergy are always produced with respect to some reference environment [5]. Reference environment can be considered as a finitely large thermodynamic body whose components are in perfect equilibrium and no work can be produced by interaction of these components. All the components have no difference in pressure, temperature, chemical potential, kinetic and potential energy. However, defining such reference environment is somewhat challenging and often the actual environment in which the process occurs is sometimes modeled as a reference environment. To overcome this difficulty some researchers have suggested a few standard reference environments for exergy analysis.

Reference environment used in this work is based on the standard environment defined by Szargut et. al [6]. The model is based on the following components at the reference temperature and pressure (T_0=298.15K and P_0=101.325kPa)

- Atmospheric gaseous components: O_2, N_2, CO_2, H_2O, O_2
- Solid reference substance of the crust of the earth;
- Ionic reference substances of the sea.

Exergy is emitted by a system when it is brought to a state of equilibrium with the environment. Restricted and unrestricted equilibriums are two degrees of equilibrium that can be achieved by a system. Later one is referred as "dead state" while the former on is mostly referred as an "environmental state". System of process is in environmental state when its temperature and pressure is similar to surroundings while dead state require full thermodynamic equilibrium (mechanical, thermal and chemical equilibrium) with the environment.

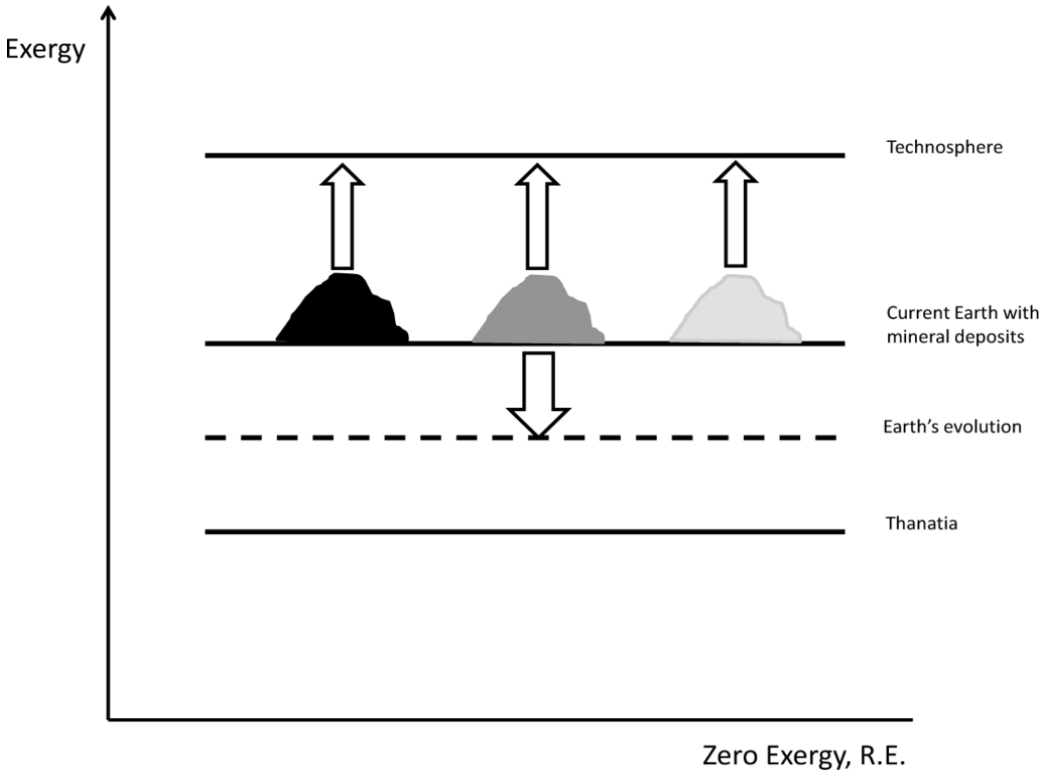

Figure 2.2: Exergy trend relative to reference environment [6]

2.3 Components of Exergy

The exergy of a matter is the maximum possible work obtainable by bringing it from its initial state through a reversible process to a state of unrestricted thermodynamic and chemical equilibrium with the environment, referred as a dead state. On a molar basis, exergy is given by [3];

$$E = E^{ph} + E^{ch} + E^{\Delta mix} \tag{2.1}$$

where E represents the molar exergy of a stream. E^{ph} is the molar physical exergy. E^{ch} is the molar chemical exergy and $E^{\Delta mix}$ is the molar exergy of mixing.

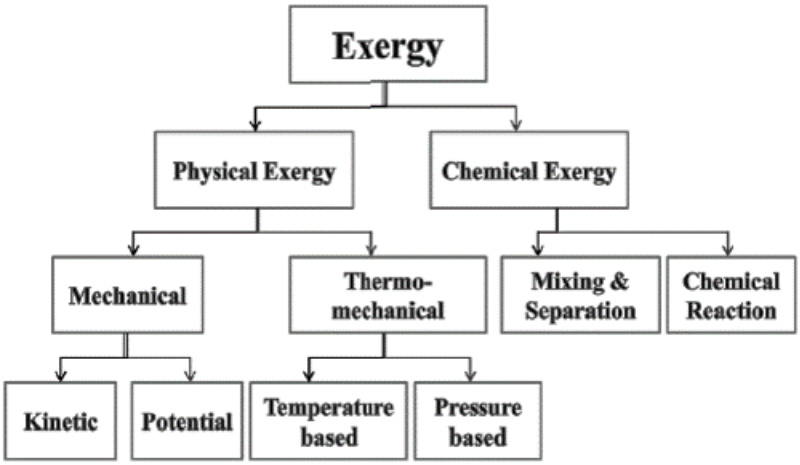

Figure 2.3: Classification of Exergy [7]

Physical exergy represents the thermo-mechanical portion of the stream's total exergy and is defined as the maximum work obtainable by taking a stream from an initial state to a state of thermo-mechanical equilibrium with the environment through physical processes only. On a molar basis physical exergy is given by [8];

$$E^{ph} = RT_0 \sum n_i ln P_i/P_0 + \sum n_i C_{Pi}^{mean} (T - T_0 - T_0 ln(T/T_0)) \tag{2.2}$$

$$C_{Pi}^{\text{mean}} = \int_{T1}^{T2} C_P dt \div \int_{T1}^{T2} dt \quad (2.3)$$

$$C_{p,j}\ (J/mol.K) = a_j + b_j T + c_j T^2 + d_j T^3 \quad (2.4)$$

where a_j, b_j, c_j and d_j are heat capacity coefficients, T_0 and P_0 is the standard temperature and pressure. P_i and T_i represents temperature and pressure of individual component at each point in the reactor.

Chemical exergy is the maximum obtainable work from a material stream by taking it from a state of thermo-mechanical equilibrium to a state of thermo-mechanical and chemical equilibrium with the environment. Chemical exergy of a material stream on a molar basis is given by [3];

$$E^{\text{ch}} = L_0 \sum_i^n x_{0,i}^l e_i^{0l} + V_0 \sum_i^n x_{0,i}^v e_i^{0v} \quad (2.5)$$

where x_i is the mole fraction of component i in the material stream and e_i is the standard molar exergy of component i. L_0 and V_0 is the liquid and vapor fraction of stream at reference temperature and pressure. Molar standard chemical exergy e_i of a chemical component is obtained from its constituents elements by [3];

$$e_i = \Delta_f G_i^0 - \sum_j v_j \bar{e}_{(\text{chem,j})}^0 \quad (2.6)$$

where $\Delta_f G_i^0$ is the standard Gibbs free energy of formation of component i, v_j is the stoichiometric coefficient of element j in chemical component i and $\bar{e}_{(\text{chem,j})}^0$ is the standard molar chemical exergy of element j.

Exergy of mixing accounts for the mixing effect arising due to isothermal and isobaric mixing of pure components at process conditions [1]. It is termed as exergy change of mixing and is negative relative to pure process components. It can be calculated by;

$$E^{\Delta mix} = \Delta_{mix} H - T_0 \Delta_{mix} S \quad (2.7)$$

where H and S are molar enthalpy and entropy of material stream at reference or environment temperature (T_0) and pressure (P_0).

A simple exergy efficiency can be calculated by the following equation [9].

$$\eta = \frac{E_{out}}{E_{in}} \quad (2.8)$$

where E_{in} represents the exergy of feed at the inlet of reactor while E_{out} is the exergy at the outlet of reactor.

2.3.1 Exergy Balances

Exergy analysis being based on both 1st and 2nd law of thermodynamics provides an important insight of degradation of energy due loss of exergy caused by irreversible nature of all the real processes. Thus, energy balance is a mathematical representation of the law of conservation of energy while the exergy balance represents the law of degradation of energy. The exergy balance of a steady state, an open volume system with constant molar flow rates is given by:

$$0 = \sum_j \left(1 - \frac{T_0}{T_j}\right) Q_j - \dot{W}_{cv} + \sum_{in} (\dot{m}_{in} E_{in}) + \sum_{out} (\dot{m}_{out} E_{out}) - \dot{E}_D \quad (2.9)$$

where T_0 and T_j represents the reference temperature and actual system temperature respectively. Q_j is the energy transferred across a control surface while $\dot{W}_{cv}$ represents the net rate of work produced by transfer of energy across a control volume. $\dot{m}_{in}$, $\dot{m}_{out}$ are the inlet and outlet molar flow rates and $\mathbf{e}_{in}$, $\mathbf{e}_{out}$ are the inlet and outlet exergy flows. $\dot{E}_D$ represents the destruction of exergy caused by entropy generation due to irreversibilities in the system.

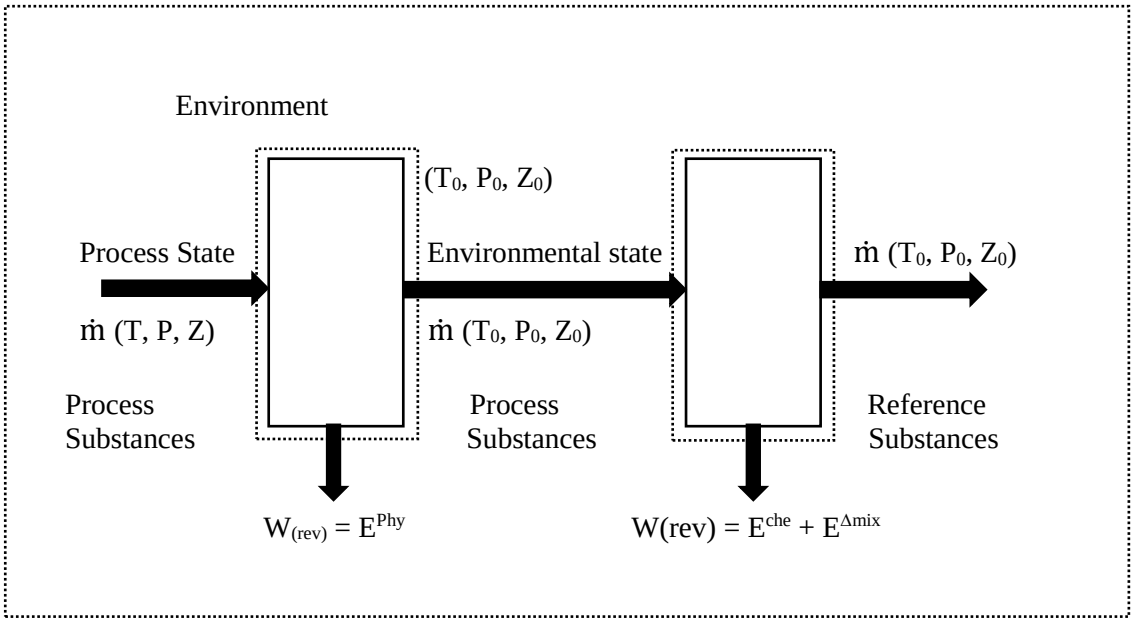

Figure 2.4: Exergy Concept. $\dot{m}$ is the molar flow rate and T, P, Z are for temperature, pressure and component respectively

2.4 Naphtha Reforming Process

Naphtha reforming process holds a key position in today's refineries due to its production of high value-added products. These products not only enhance the capacity of the gasoline pool by the addition of high octane number reformate, but also serves as a valuable raw material (butane, toluene and xylene) for petrochemical industry. Hydrogen is also a potential by product of reforming process that is utilized in several hydrotreating processes like hydrogenation, hydrodesulphurization etc. Naphtha is a complex mixture of 300 plus hydrocarbons with carbon atoms ranging from one to twelve and having boiling points in the range of 30 to 200^0C and occupies 15-30% of crude oil. As shown in Fig. 2.5, naphtha is typically composed of four major hydrocarbon groups; iso-Paraffins, Naphthenes, Aromatics, n-Paraffins. The main purpose of a reforming process is to increase the percentage of aromatics in order to boost the octane number of the reformate.

Naphtha reforming processes can be categorized as semi regenerative, cyclic and continuous regenerative depending on the mode of catalyst regeneration. Continuous catalyst regeneration (CCR) process, due to its advantages, is now a more widely used technique in newly developed naphtha reforming units. Production of high octane

reformate, operations at lower temperatures, high purity hydrogen production and low recycle ration are a few of the many advantages of CCR process over traditional naphtha reforming processes. Fig. 2.6 shows major components of a continuous catalytic regenerative (CCR) process for naphtha reforming, which includes multiple adiabatic reactors in side-by-side arrangement, a catalyst regeneration unit and product separators. The size of the reactors increases progressively where first reactor being the smallest while the last being the largest of all. Hydrotreated naphtha feed along with recycled hydrogen and catalyst particles flows in a cross row arrangement from first to the last reactor. After the last reactor, catalyst particles are regenerated and sent back to the first reactor. While the reformed stream from the reactors are sent to product separators to strip off hydrogen and other light gases from it.

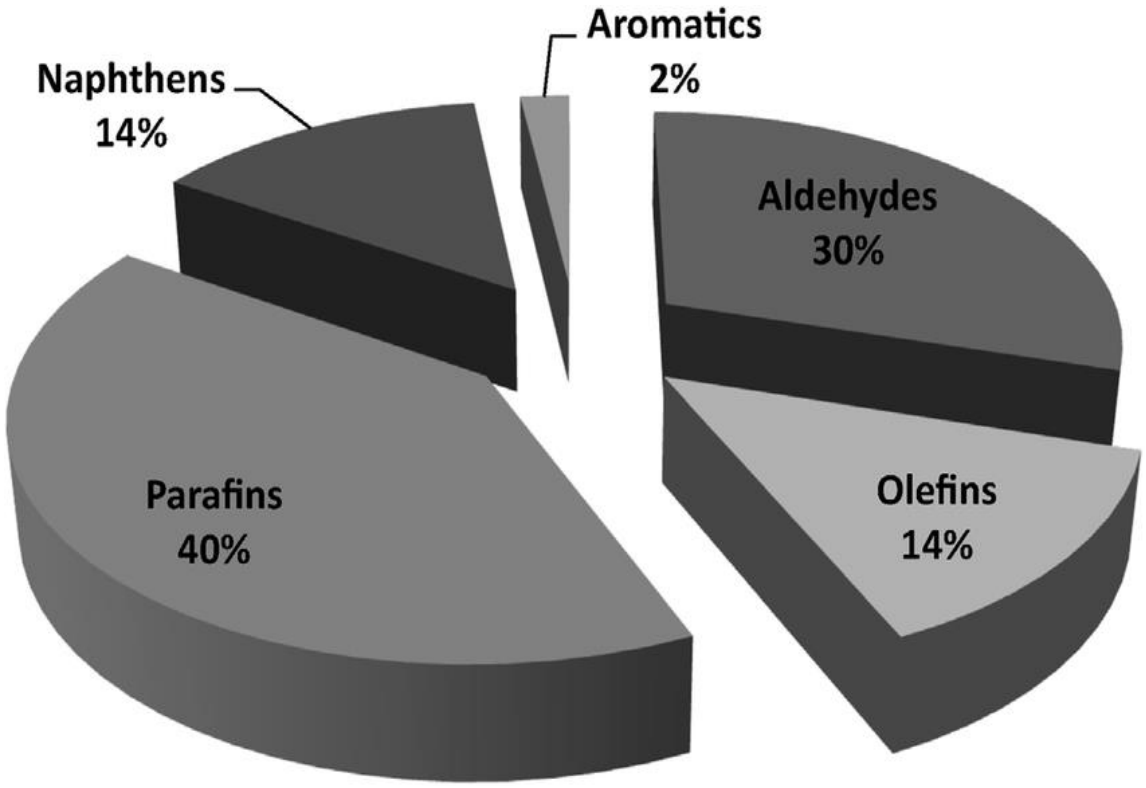

Figure 2.5: Composition of Naphtha [10]

2.4.1 Importance of Exergy Calculation in Naphtha Reforming Process

For a better catalyst activity and output field, naphtha reforming processes are usually done at a higher optimal temperature. However, due to the endothermic nature of reforming reactions, interstage heating is required to maintain that optimal reaction temperature making the process highly energy intensive, it is desired to increase the energy efficiency of the process to make it more feasible and sustainable, in this regard exergy analysis can be helpful in locating and quantifying the sources of irreversibilities in the process that are associated with energy losses. Once identified, process can be rectified to minimize these losses making it much more energetically feasible [11].

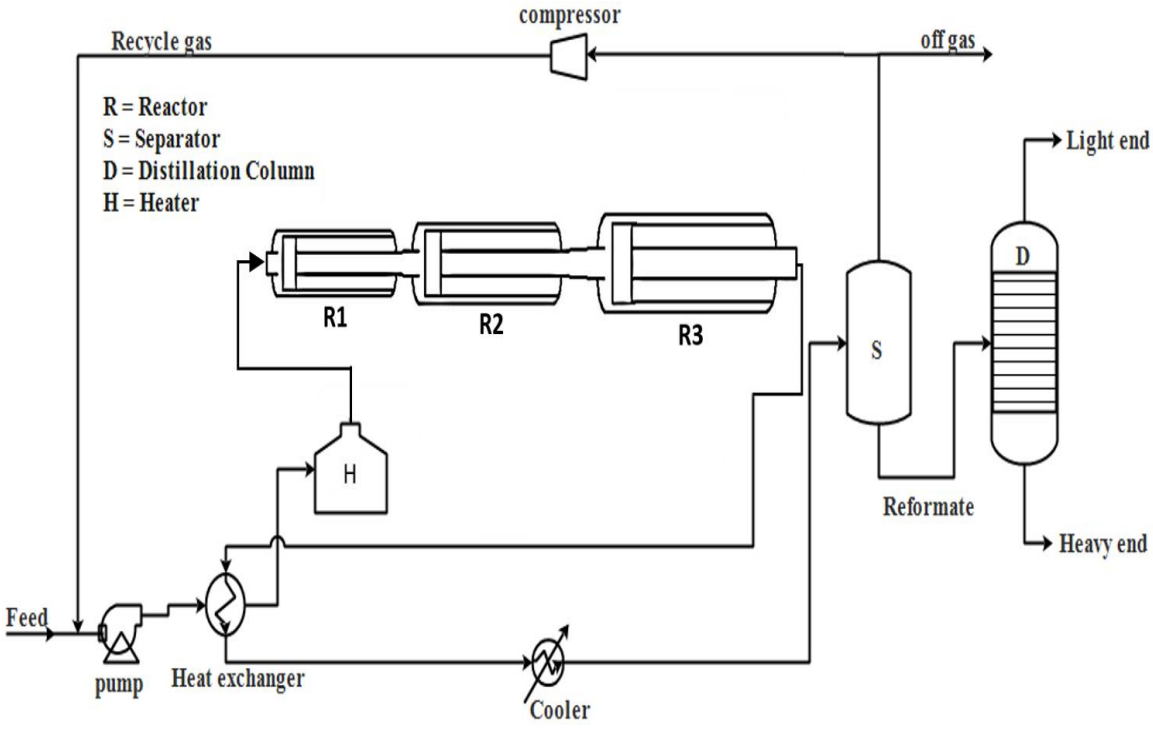

Figure 2.6: Block diagram of a naphtha reforming plant

2.4.2 Reaction kinetics of naphtha reforming process

The categories of reactions modeled in this process include n-heptane isomerization, iso-heptane dehydrogenation, naphthalene dehydrocyclization and naphthalene hydrocracking which are shown in Table 1.

In isomerization, the transformation of one molecule into another molecule takes place through the different arrangement of atoms but total no of atoms remains constant. Dehydrogenation removes hydrogen molecule to increase the aromaticity and produce more reactive components. Dehydrocyclization reaction converts naphthenic component into an aromatic component by removal of hydrogen. The rate of dehydrocyclization reaction is slower than dehydrogenation and mainly takes place in the second and third reactor. Hydrocracking mostly takes place in the third reactor and has slow reaction rate. It utilizes hydrogen to break heavier molecule, producing lighter components which reduces the reformate yield.

Table 2.2: Types of naphtha reforming reactions and reaction kinetic parameters [12]

Reactions	Category	Pre-exponential factor	Activation energy (cal/mol)
n-Heptane ⇢ iso-Heptane	Isomerization	3.08×10^{8}	40000
iso-heptane ⇢ Naphthalene	Dehydrogenation	3.04×10^{8}	30000
Naphthalene ⇢ Toluene	Dehydrocyclization	1.37×10^{10}	45000
Naphthalene ⇢ Cracking Products	Hydrocracking	1.61×10^{13}	53000

Chapter-3

Computational Fluid Dynamics Based Modeling

Computational fluid dynamics is a subdivision of fluid dynamics which uses data structure and numerical analysis to analyze and solve problems based on fluid flow. To perform the calculations, computers are required to simulate the gases and liquids interaction with surfaces described by boundary conditions. Better solutions can be achieved through high speed supercomputers. Through continuous research, many softwares are developed which can enhance the speed and accuracy of complex simulation problems such as turbulent and transonic flows. These softwares are validated by experimental comparison using wind tunnel and final validations are done by flight tests.

3.1 Background

Navier-Stokes equations are the fundamental basis of all CFD problems and these equations define many single-phase fluid flow problems. To simplify these equations, viscous terms are removed to yield the Euler equations. To simply further these equations and yield potential equations, vorticity terms are removed. Finally, linear potential equations are obtained by removing the subsonic and supersonic flow terms.

Earlier Lewis Fry Richardson divided the physical space into cells and apply finite different method which resembles with modern CFD calculations. Although he failed to get the required results but latter these calculations which he mentioned in his book "Weather prediction for numerical process" provide the basis for modern CFD calculations.

3.2 Methodology

3.2.1 Preprocessing

The preprocessing consists of the following steps:

- Computer aided design (CAD) can be used to defined the physical bound and geometry of problem. From there, fluid volume is extracted.

- The volume which is occupied by fluid is then divided into discrete cells (mesh). The mesh may be uniform or non-uniform, pyramidal or polyhedral, tetrahedral, structure or unstructured cells.
- Now the physical mesh is defined using fluid motion, radiation, enthalpy and species conservation or non-conservation equations.
- Boundary conditions are specified.

3.2.2 Processing

Simulations are processed until the convergence is reached and the different equations are solved as steady state or transient.

3.2.3 Post processing

Finally, the post processing is done to aid the visualizing and analysis of the solution.

3.3 Simulation Environment

3.3.1 Gambit 2.4.6

There are many geometries making softwares such as Gambit, Solid works, Auto CAD, IGES etc. Gambit is most basic and user-friendly software compare to others. So, Gambit 2.4.6 is used to prepare geometry. In this work, two-dimensional geometry is prepared with the help of vertices. Vertices are connected with each other to form the edges which can be further used to form faces. Unstructured meshes are prepared and boundary conditions are labelled at edges while different zones are labelled at faces. Errors in geometry is resolved through bottom console of Graphical user interface (GUI). GUI of Gambit 2.4.6 is shown as,

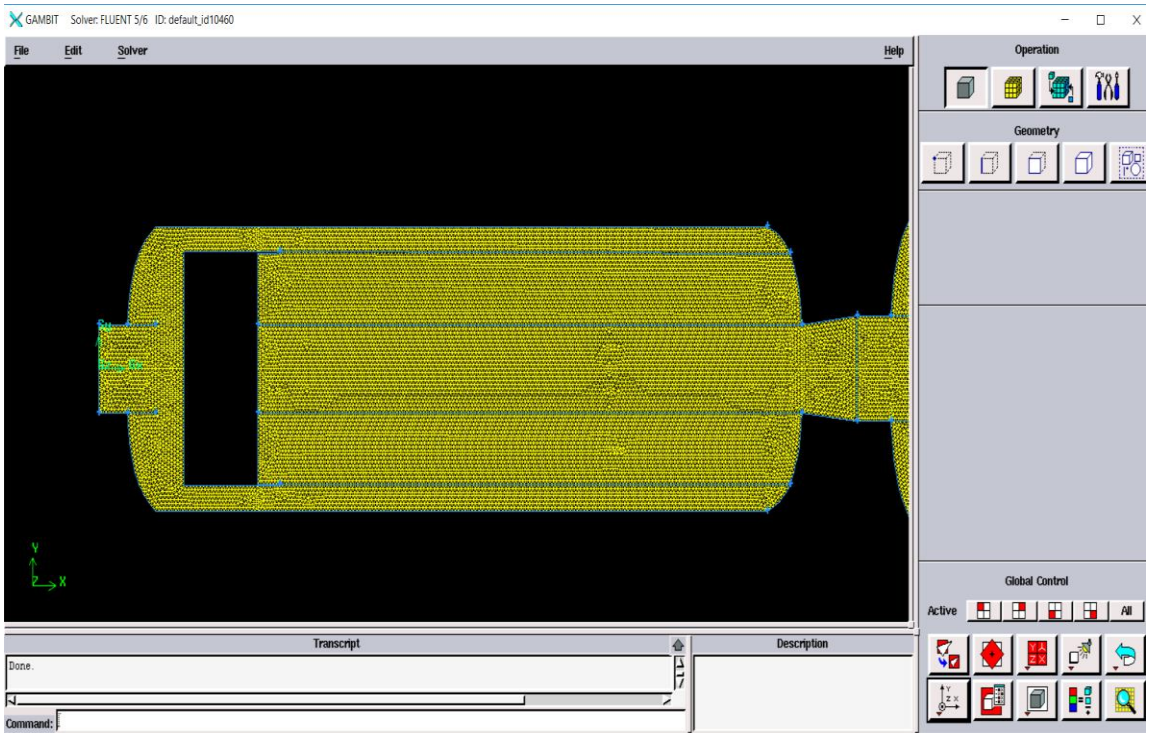

Figure 3.1: Radial flow reactor geometry

3.3.2 ANSYS Fluent

Geometry is exported from Gambit to the Fluent software which performs required simulation. Control volume method is used to solve the mass, energy and species conservative equations. Mesh quality is calculated in ANSYS fluent. The boundary and zone conditions which are labelled in Gambit software are now specified one by one in Fluent. Under solution method, pressure velocity coupling scheme is chosen and specified the spatial discretization for gradient, pressure, momentum, turbulent kinetic energy, turbulent dissipation rate and species. Under solution control method, relaxation factors are adjusted for pressure, velocity, density and other parameters. Residual monitors for absolute convergence are specified to find out the absolute convergence. After that initialization of solution is done and then iteration is performed at different equations until the absolute convergence is achieved. Figure 3.2 shows the GUI of fluent tool.

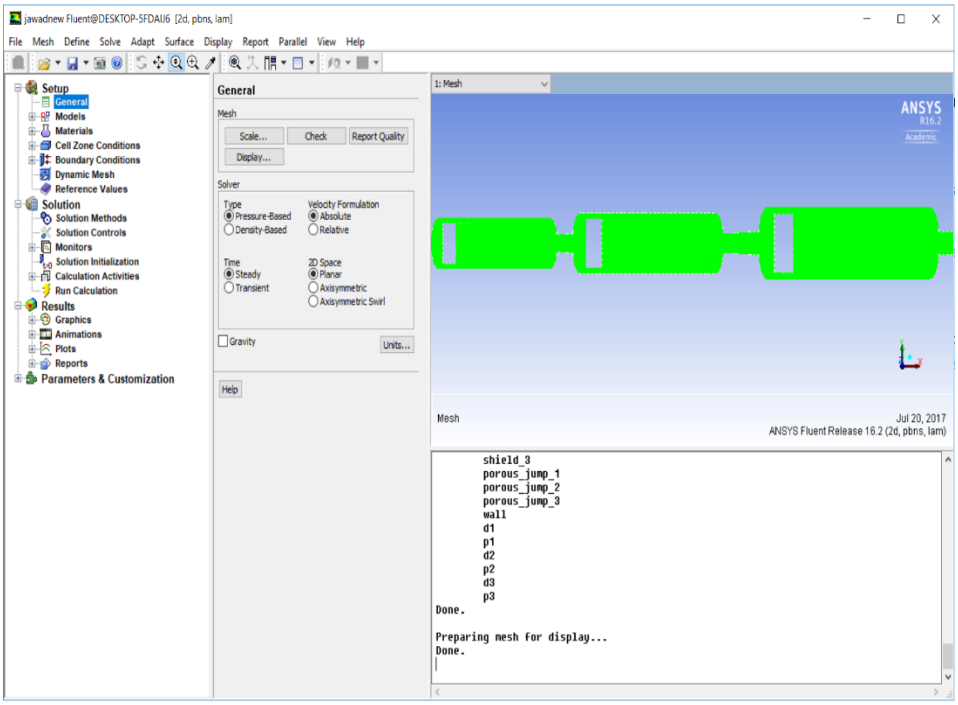

Figure 3.2: ANSYS Fluent Environment

Four reaction models; laminar finite-rate, finite-rate/eddy-dissipation rate, eddy-dissipation and eddy-dissipation concept are present in the fluent to deal with reactions and incorporate turbulence-chemistry interactions. In laminar finite-rate, Arrhenius expressions are used to calculate reaction rate and turbulence effects are ignored. In finite-rate/eddy-dissipation rate, both Arrhenius expression and mixing can influence the reaction. The smaller value among Arrhenius rate and mixing rate is considered the rate of reaction. In eddy-dissipation model, the reaction rate is controlled and determined by turbulence while in eddy dissipation concept model, Arrhenius expression is also incorporated in turbulent flames. Laminar finite-rate model is not recommended in turbulent conditions due to non-linearity in Arrhenius chemical kinetics. The values of different reaction parameters in these reaction models which includes pre-exponential factor, activation energy, mixing law constants, stoichiometric coefficients and rate exponent are required to incorporate different reactions as shown in these figures.

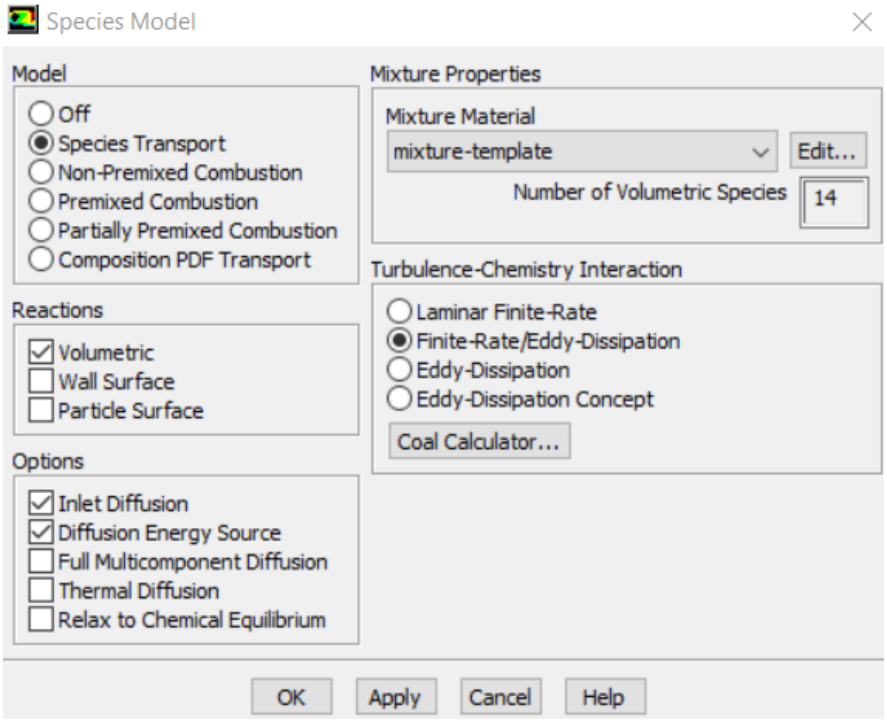

Figure 3.3: Reaction models

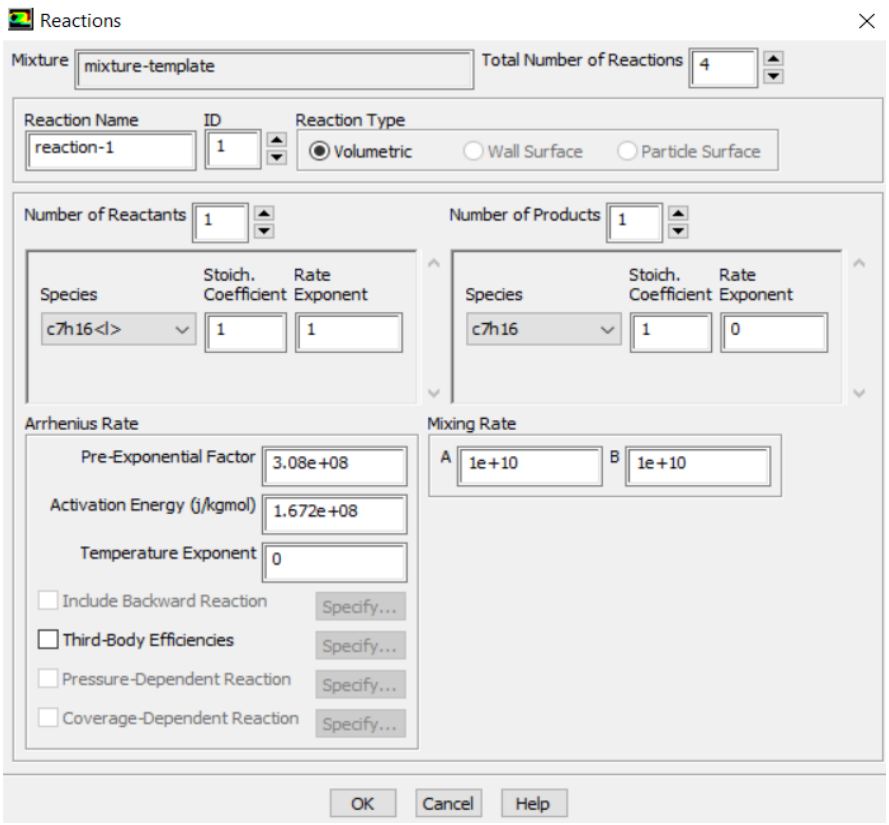

Figure 3.4: Reaction parameters

3.3.2.1 ANSYS Fluent interfacing with C language

Computational fluid dynamics are basically developed for aerodynamics and mechanical engineers to analyze the stress and strain analysis of different equipment under different conditions. To solve the problem of chemical engineering in CFD, some components and reactions are not present in the database of Ansys Fluent which required the external interface through coding. C language is used in this case to build an interface with the ANSYS fluent to insert the species and reaction properties and this is shown figuratively in the following figures.

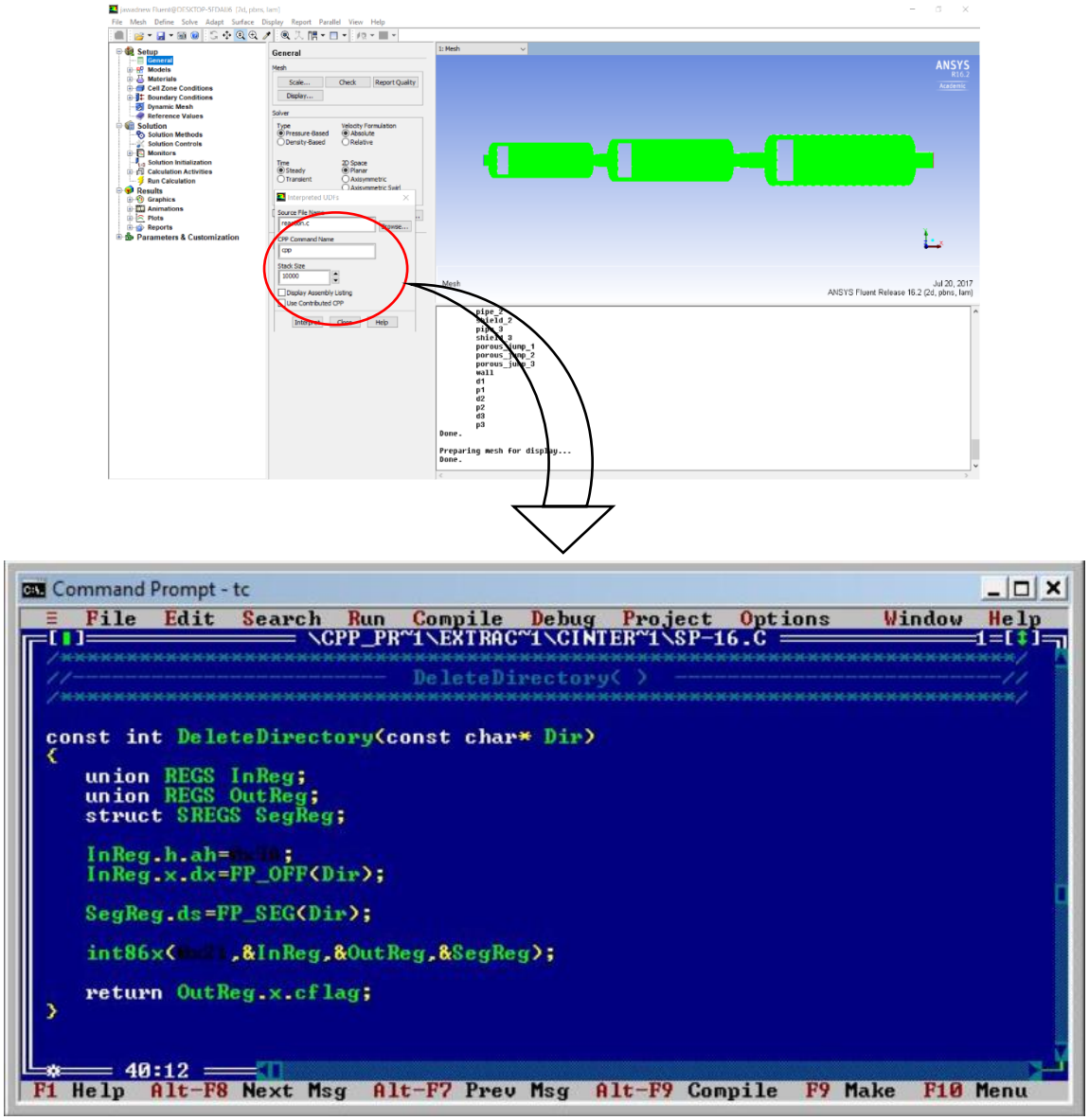

Figure 3.5: ANSYS fluent interfacing with C language environment

3.3.2.2 Convergence criteria

The commonly used absolute convergence criteria for the residuals of continuity, x-velocity, y-velocity, epsilon and species equation is .001 while the convergence criteria is 1e-06 for energy equation. To achieve the convergence, the absolute convergence criteria needs to be satisfied.

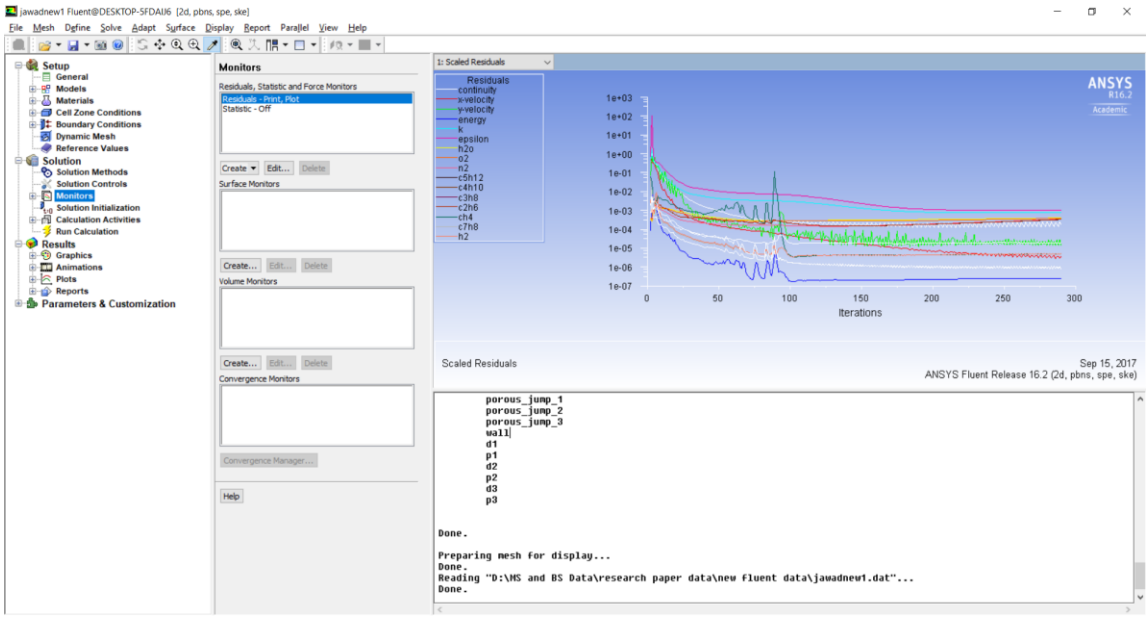

Figure 3.6: Iterations

3.4 Applications of Computational fluid dynamics modeling

CFD has different applications in different fields

- In architectural field, it is used to design comfortable and safe environments
- It is used by vehicle's designers to improve aerodynamic features
- CFD is very helpful in the analysis of drug delivery
- Military equipment can be designed by using this technique
- Petroleum engineers used this technique to developed oil recovery strategies

Chapter-4

Literature Review

This chapter includes the discussion regarding the computational fluid dynamic (CFD) based exergy analysis of different processes. Hydrodynamic analysis of naphtha reforming reactors is explained. Comparison of CFD approach with the already established technique like Aspen Plus is also discussed in this chapter.

4.1 Computational fluid dynamics technique to quantify Exergy

Exergy analysis as compared to the energy analysis presents the true picture of energy conservation and quantification. Computational fluid dynamics is a latest technique which can achieve this in a microscale. Yong-an, et al. (2009) performed exergy analysis to measure the exhaust emissions of gases from kitchen and finds the similarity between the exergy and concentration analysis. Exhaust gases are major air pollutant which is responsible of about 30% of world health problems. To predict the degree of pollution from exhaust gases is very important to limit its emissions. Exhaust gases mainly consists of carbon monoxide and carbon dioxide and with computational fluid dynamics (CFD) simulations incorporating exergy phenomena can predict the distribution of these gases. Exergy represents the work potential of a system. In the case of exhaust emission of gases, it represents the harmful effects that system occupying these gases projects on the environment. To incorporate exergy analysis in CFD interface in build in the C language and it is inserted into the CFD software as user defined function. PISO algorithm is used to solve conservative equations while K-epsilon model is used to deal with the turbulence. Percentage of CO_2 is maximum near to the ignition source because maximum combustion takes place at this point while CO percentage is minimum near the ignition source. As we go further from ignition source CO_2 percentage deceases and increase in CO percentage takes place which is due to the slower combustion process and maximum conversion of CO_2 to CO. At near the ignition point value of exergy is maximum and decreases as we move away from the source. So, CFD can deal the system in a micro level and

incorporating exergies can predict help us to determine the work potential at every point [13].

Farmahini–Farahani (2012) performed exergy analysis to study the thermal stratification process in a storage tank. Thermal stratification is the layering of water in which hot water comes at top due to low density while high density stays cold water at bottom. Geometrical parameters of tank like inlet and outlet position, inlet angle, aspect ratio and inlet and outlet diameter can effect on level of thermal stratification which can predict through exergetic trends. Thermal stratification is very important industrial phenomena and exergetic analysis can contribute to the optimum design of storage tank [14].

Boulenouar and Ouadha (2015) performed exergy analysis to identify the loss areas in a steam ejector in refrigeration system. Compressible flow is assumed and conservative equations are solved through finite volume method. To deal with turbulence in a system, K-ω turbulence model is introduced. Steam ejector consists of nozzle, throat, diffuser and mixing chamber. Major exergy losses occur in the nozzle due to high velocity and pressure gradients [15].

Alabi and Ladeinde (2007) performed exergy analysis through CFD to optimize the aircraft. Exergy analysis identify the areas of exergy destruction and provide room for designer to improve the design of aircraft. The results show that exergy destruction and entropy generation is higher on the top part of the aircraft due to maximum velocity gradient compared to lower portion of aircraft. The CFD based results are compared with the lumped parametric model. CFD gives more accurate prediction of exergy analysis than lumped parametric model but it takes more time [16].

Jafarmadar (2015) performed exergy analysis to control combustion timings of fuel blends in which fuels have different ignition properties. It is observed that exergetic efficiency of compressed natural gas is higher than gasoline fuel which shows that CNG has higher work potential. It is also found that exergetic efficiency decreases when fuel-air ratio increases. This is due to the fact that excessive combustion increases the percentage of carbon dioxide which has low heating value. Hence overall heating value of products decreases which lowers the fuel work potential [17].

4.2 Hydrodynamics study through computational fluid dynamics approach

To determine the flow distributions and pressure drop in packed bed (filters) CFD approach can be very useful. A packed bed filter has non-uniform distribution of voids. Taylor, et al. (1999) developed a computational model in CFD to analyze to effects of pressure on the void distribution by incorporating the Mueller equation. To deal with turbulence in the bed, standard K-epsilon (two equations) turbulence model is used. A pressure loss is observed in the bed which is determine with the help of Ergun equation. Through this model, an efficient bed filter can design in which optimum flow distribution is achieved [18].

Membrane reactor is a latest technology to remove nitrogen, organic materials and other waste water contaminants from water. CFD is a promising approach to improve the performance of membrane reactor. Efficiency of membrane reactor rely on mass transfer phenomena which depends upon flow patterns and flow velocity. A tubular hollow membrane is used and a stimulus response approach is used to investigate the flow patterns. Plascencia-Jatomea, et al. (2015) developed a CFD based model by assuming laminar flow and solve navier stokes equation for incompressible flow. A deviation from ideal hydrodynamic behavior is observed due to mixed flow and channeling effects. With the velocity flow patterns, stagnant zone is determined in the membrane in which degradation reactions can take place [19]. This stagnant zone can provide the room for improvement of membrane reactor design.

Naphtha reforming is a very complicated process as it involves hundreds of hydrocarbons and their reactions. To improve the internal hydrodynamics of naphtha reforming reactors is very important to obtain fuel which have high research octane number (RON). Hydrodynamics of naphtha reforming process mainly includes catalytic porosity of bed, flow regimes and pressure drop across each reactor. Recirculation effects and vortices are observed in first reactor which create pressure drop and is minimized through CFD modeling. Bed porosity is optimized through pressure drop measurement at different porosity level. Pressure drop that is obtained from CFD modelling is compared with Ergun equation. Mainly pressure drop occurs in shield and heat distribution area. Screen and heat

distribution redesign can significantly reduce the overall pressure drop across the three reactors [20, 21].

4.3 Exergy analysis through different tools and their comparison with CFD

Process design intensively involves process simulators such as Aspen HYSYS/PLUS, CHEMCAD, etc. However, the simulators lack in built-in robust mechanism for exergy analysis that can be applied to any process being designed. In order to overcome this deficiency, exergy analysis tools are developed in other environments such as FORTRAN, Microsoft Excel, etc., and interfaced with the simulators for analyzing exergy efficiency of the designed process. Querol et al. (2011) integrates Microsoft Excel with Aspen PLUS to calculate exergy and performed exergoeconomis studies of chemical processes [22]. Montelongo-Luna et al. (2011) developed relative exergy array (REA) to measure the exergetic efficiency of distillation column [23]. Munir et al. (2013) developed relative exergy-destroyed array (REDA) to evaluate the eco-efficiency of the monochlorobenzene (MCB) plant and a heat exchanger network (HEN) [24]. Hinderink et al. (1996) studied exergy analysis by developing a tool in which an external subroutine (Exercom) is integrated with flowsheeting simulator Aspen PLUS to incorporate the standard chemical exergies of components [3]. Bahmanpour et al. (2014) studied the conversion of natural gas to methanol and methanol to formaldehyde, exergy analysis is performed using Aspen HYSYS and Aspen PLUS [25].

Computational fluid dynamics (CFD) technique is the latest emerging approach to performing exergy analysis of a given system [13, 14]. CFD provides an internal visualization aid compared to other techniques, i.e. Aspen HYSYS/PLUS, CHEMCAD, etc., in which only inlet and outlet exergies are calculated. Huang et al. (2017) investigated the exergy analysis of crystalline nickel ferrite dissociation in a solar reactor and figured out that physical exergy decreases with temperature drop. It was noted that high conversion rate of reaction increases the oxygen production which results in increase of chemical exergy of the process [26]. For naphtha Reforming process, a CFD-based hydrodynamic analysis has been performed [27]. However, to the best of our knowledge, no CFD based exergy analysis is reported in naphtha reforming process.

4.4 Objectives

In this study, a CFD-based technique for exergy analysis of naphtha reforming reactors is developed. In order to incorporate reaction kinetics of naphtha reforming process; an interface is created with C language through an extension. N-heptane fraction is used as a representative of the several hundred hydrocarbon components involved in the naphtha reforming reactions. The lumped reaction kinetics approach is adopted to provide required information of the isomerization, dehydrogenation, dehydrocyclization and hydrocracking in CFD.

Table 4.1: Summary of literature survey

Year	Auther	Work done	Method used
2009	D. Iranshahi et al	Modeling of naphtha reforming unit applying detailed description of kinetic in continuous catalytic regeneration process.	MatLab
2011	E. Querola et al	Novel application for exergy and thermoeconomic analysis of processes	Aspen Plus simulation
2012	H Abdallah et al	Exergetic optimization.	Aspen Plus and Matlab
2013	Mohammadikhah et al	Improvement of Hydrodynamics Performance of Naphtha Catalytic Reforming Reactors.	Computational Fluid Dynamics (CFD)
2013	Ao Yong-an et al	Exergy analysis of Exhaust-gas of Burning Liquefied-Gas in A Chinese Kitchen.	Computational Fluid Dynamics (CFD)
2014	Bahmanpour et al	Exergy analysis of natural gas to methanol and methanol to formaldehyde conversion	Aspen HYSYS and Aspen PLUS
2017	Huang et al	exergy analysis of crystalline nickel ferrite dissociation in a solar reactor	Computational Fluid Dynamics (CFD)

Chapter-5

Model Development

Gambit 2.4.6 is used to create geometry and mesh, and ANSYS Fluent 16.2 is used to simulate the process. In section 5.1, details regarding geometry and mesh preparation are provided while in section 5.2, identification of boundary and cell zone conditions is mentioned. A set of CFD based conservative equations is referred in section 5.3 and to solve these equations different numerical schemes are used which are given in section 5.4. Following are the assumptions for model development:

- Equilibrium state is reached and maximum yield is achieved.
- Coking reaction is ignored and temperature of the reactor contents is assumed to be the same to the temperature of inside wall of the reactor.
- Heat flux and radiation properties of the gases remain constant.
- There is negligible heat loss from the wall of reactors to the surroundings.
- Reactions are assumed to be in homogenous phase

5.1 Geometry and Meshing

The geometry of three radial reactors is constructed in two dimensions where unstructured elements of a mesh form a triangular shape. The geometry consists of the annulus, catalytic bed, and a central pipe. Gases pass through annulus region into the catalytic bed and moved out through the central pipe, Fig. 5.1. The three important parameters to evaluate the mesh quality are minimum orthogonal quality, maximum Ortho-Skew and maximum aspect ratio having values 0.543314, 0.229389 and 4.13232, respectively. Fig. 5.1 identifies the path of reactants through fixed bed. Fig. 5.2 shows the dimensions of reactors in which height and length of packed bed, central pipe and annulus increases from reactor 1 to reactor 3. In Fig. 5.3, a computational grid of naphtha reforming reactors is shown. Table 5.1 presents the mesh characteristics such as minimum volume, maximum volume, total volume, no of elements, wedges, minimum face area and maximum face area. The total volume is summation of volumes of all triangular cells present in geometry.

distribution redesign can significantly reduce the overall pressure drop across the three reactors [20, 21].

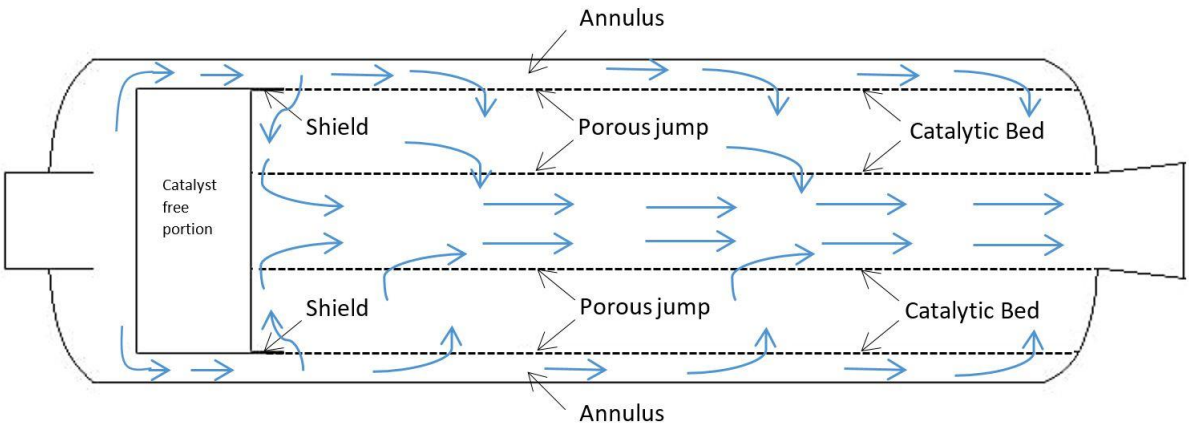

Figure 5.1: Flow path of gases in reactors

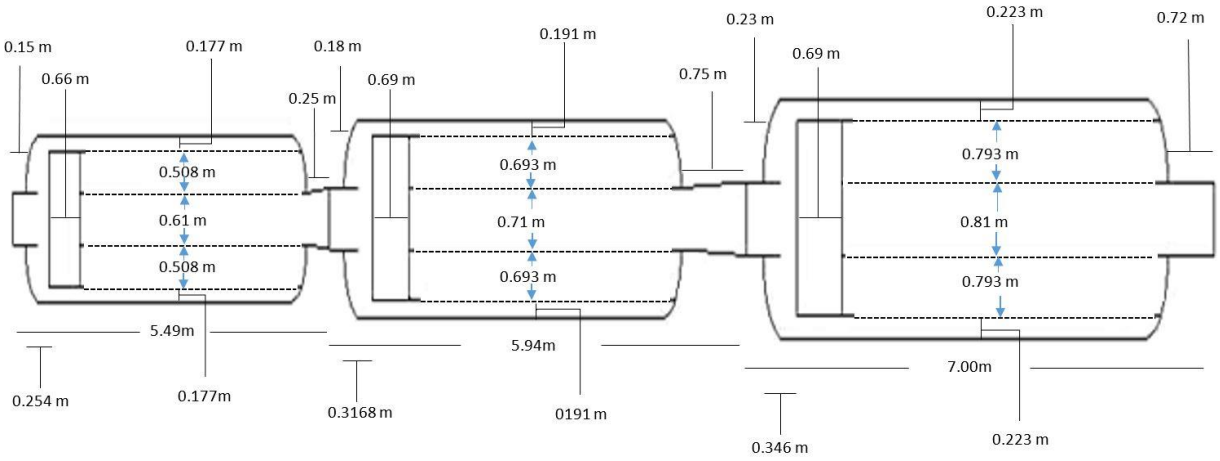

Figure 5.2: Dimensions of the catalytic reactors

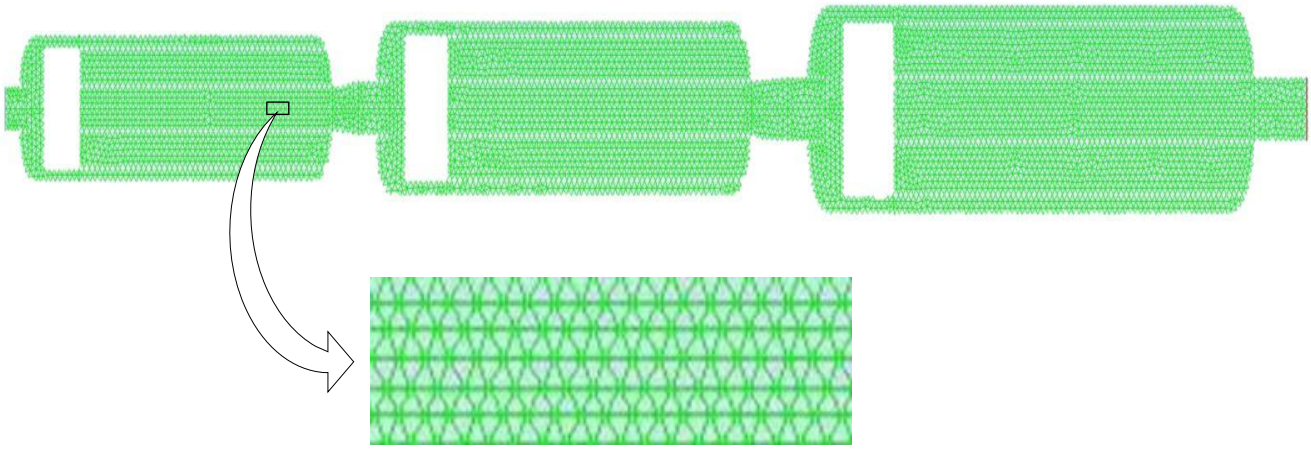

Figure 5.3: Computational grid of Reactors

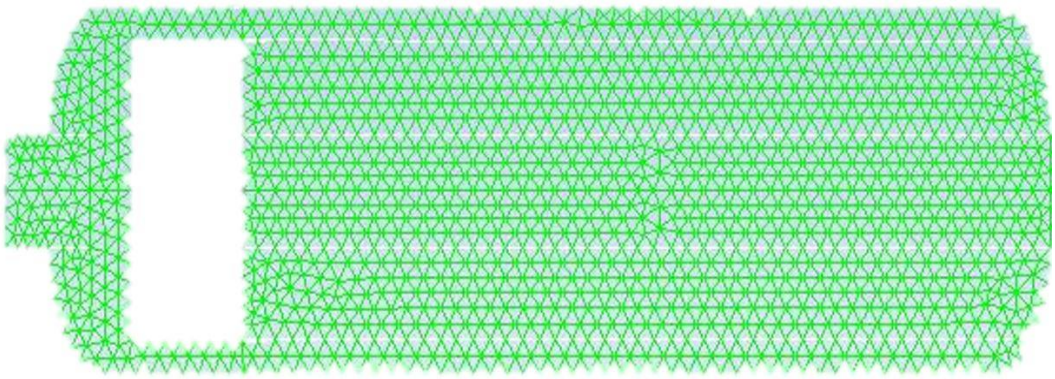

Figure 5.4: Computational grid of Reactor 1

Table 5.1: Values of different mesh properties

Properties of mesh	Values
Orthogonal quality (Minimum)	5.43314e-01
Ortho skew (Maximum)	2.29389e-01
Aspect ratio (Maximum)	4.13232
No of Nodes	132982
No of elements	125612
Wedges	125612
Minimum volume (m3)	1.941511e-04
Total volume (m3)	5.134194e+01
Minimum face area (m2)	1.650226e-02
Maximum face area (m2)	4.221791e-02
Maximum volume (m3)	6.186525e-04

5.2 Boundary and Cell Zone Conditions

Boundary conditions were defined for inlet of reactor 1 and outlets of reactor 3. Besides, a porous jump condition is applied to a model pressure drop within the reactor geometry. The porous jump condition of all the three reactors is specified through permeability and inertial loss coefficient. For packed bed designing, three porous zones and three fluid zones are used in total. The porous zones are used to specify the values of inertial resistance and viscous resistance in the packed bed. Temperature and pressure specifications of inlet and outlet boundary conditions are given in Table 5.2 and 5.3, respectively. Paraffinic naphtha feed is made up of n-paraffin, iso-paraffin and cyclo-alkane as identified in Table 4. Paraffinic nature of feed lowers the octane rating. After processing through reactions, octane number is improved by converting the paraffin to aromatics and light hydrocarbons.

Table 5.2: Temperature and Pressure at inlet and outlet

Boundary condition	Temperature (K)	Pressure (Pa)
Inlet	811	2790120
Outlet	744	2774900

Table 5.3: Components mole fraction at inlet and outlet

Boundary condition	Components mole fraction		
	n-heptane	CH3C6H11	Iso-heptane
Inlet	0.55	0.33	0.12
Outlet	0.2	0.004	0.07

5.3 CFD conservative equations

Finite volume method with cell centered configuration is used to discretize the species, energy, continuity and momentum equations. Computational control volumes are used to demonstrate the conservation laws. Conservation laws are executed on each control volume and across the domain using species transport, energy conservative, continuity, and momentum equation.

5.3.1Species transport equation

$$\frac{\partial(\rho Y_{\mathrm{i}})}{\partial t} + \nabla.(\rho \vec{v} Y_{\mathrm{i}}) = -\nabla.\vec{J}_{\mathrm{i}} + R_{\mathrm{i}} + S_{\mathrm{i}} \quad (4.1)$$

where Y_i is a mass fraction of species, S_i is creation rate of species and R_i is net production rate of species through chemical reactions

5.3.2 Energy conservative equation

$$\frac{\partial(\rho E)}{\partial t} + \nabla.\left(\vec{v}(\rho E + p)\right) = -\nabla.\left(\sum_{\mathrm{j}} h_{\mathrm{j}} J_{\mathrm{j}}\right) + S_{\mathrm{h}} \quad (4.2)$$

where S_h represents volumetric heat source, h_i is the enthalpy, p is local static pressure and J_i describe the flux coming out of control volume.

5.3.3 Continuity equation

$$\frac{\partial \rho}{\partial t} + \frac{\partial(\rho v_x)}{\partial x} + \frac{\partial(\rho v_r)}{\partial r} + \frac{\rho v_r}{r} = S_m \tag{4.3}$$

where S_m represents mass addition to the continuous phase

5.3.4 Momentum equation:

Momentum equations in axial and radial direction are as follows:

$$\frac{\partial(\rho v_x)}{\partial t} + \frac{1}{r}\frac{\partial(r\rho v_x v_x)}{\partial x} + \frac{1}{r}\frac{\partial(r\rho v_r v_x)}{\partial r} = -\frac{\partial \rho}{\partial x} + \frac{1}{r}\frac{\partial}{\partial x}\left[r\mu\left(2\frac{\partial v_x}{\partial x} - \frac{2}{3}(\nabla.\vec{v})\right)\right] + \frac{1}{r}\frac{\partial}{\partial r}\left[r\mu\left(\frac{\partial v_x}{\partial r} + \frac{\partial v_r}{\partial x}\right)\right] + F_x$$

(12)

$$\frac{\partial(\rho v_r)}{\partial t} + \frac{1}{r}\frac{\partial(r\rho v_x v_r)}{\partial x} + \frac{1}{r}\frac{\partial(r\rho v_r v_r)}{\partial r} = -\frac{\partial \rho}{\partial r} + \frac{1}{r}\frac{\partial}{\partial x}\left[ru\left(2\frac{\partial v_r}{\partial r} - \frac{2}{3}(\nabla.\vec{v})\right)\right] + \frac{1}{r}\frac{\partial}{\partial x}\left[ru\left(\frac{\partial v_r}{\partial x} + \frac{\partial v_x}{\partial r}\right)\right] - 2\mu\frac{v_r}{r^2} + \frac{2}{3}\frac{\mu}{r}(\nabla.\vec{v}) \quad + \rho\frac{v_{z^2}}{r} + F_r$$

(13)

where

$$\nabla.\vec{v} = \frac{\partial v_x}{\partial x} + \frac{\partial v_r}{\partial r} + \frac{v_r}{r} \tag{4.4}$$

$$F_i = -\left(\sum_{j=1}^{3} D_{ij}\mu v_j + \sum_{j=1}^{3} c_{ij}\frac{1}{2}\rho|v|v_j\right) \tag{4.5}$$

$$F_i = -\left(\frac{\mu}{\alpha}v_i + c\frac{1}{2}\rho|v|v_i\right) \tag{4.6}$$

Ergun equation is used to compute pressure drop by means of a correlation containing velocity, sphericity, porosity, pellet diameter, fluid viscosity and density (Ergun, 1952 , Metha and Hawley, 1969).

$$\frac{\Delta P}{L} = \frac{150\mu}{D_p^2\phi_p^2}\frac{(1-\varphi)^2}{\varphi^3}v + \frac{1.75\rho}{D_p\phi_p}\frac{(1-\varphi)}{\varphi^3}v^2 \tag{4.7}$$

$$\frac{\Delta P}{L} = \frac{\mu}{\alpha} v + \frac{1}{2} c \rho v^2 \tag{4.7}$$

where D_p is pellet diameter, ϕ_p is sphericity and φ represents porosity.

5.3.5 Inertial loss coefficient and permeability (Pamuk and Özdemir, 2012)

$$C = \frac{3.5}{D_p} \frac{(1-\varphi)}{\varphi^3} \tag{4.9}$$

$$\alpha = \frac{D_p^2}{150} \frac{\varphi^3}{(1-\varphi)^2} \tag{4.10}$$

5.4 Numerical Schemes

Finite volume method is applied on an unstructured grid to discretize the integral nature of the governing equations i.e. momentum, energy, continuity, and species conservation. To deal with turbulence, a semi-empirical two-equation model, i.e., standard k-epsilon, is used which is simple and experimentally proven. SIMPLE (Semi-implicit Method for Pressure Linked Equations) algorithm is used for pressure-velocity coupling. Discretization of pressure correction and momentum equation is solved implicitly while velocity correction is solved explicitly. Green gauss cell based gradient is evaluated using the face value which is the arithmetic average of the values at the adjoining cell centers. Standard interpolation scheme interpolates the values of pressure at the faces while the first order upwind scheme solves turbulent kinetic energy and turbulent dissipation rate. Second order upwind scheme solves momentum and species conservative equations. Under-relaxation factor is used to slow down the rate of change. The values used for pressure, momentum, turbulent kinetic energy, turbulent dissipation rate and species are 0.3, 0.7, 0.8, 0.8 and 1, respectively. The default reference frame, relative, is used for velocity initialization. Bed porosity of 0.3 is used which gives optimum pressure drop and proper residence time for reaction kinetics. As the Mach no is not that high due to low velocity so compressibility effects are ignored and a pressure based solver is used. Furthermore, finite rate formulation is enabled for calculating the reacting flow. Finite-Rate/Eddy-Dissipation model is used for turbulence-chemistry interaction. Due to the high values of mixing rate coefficients, Arrhenius rate becomes the controlling factor. The pellet diameter is 0.0015 m and its sphericity is 1

Model development starts with geometry composition preceded by mesh preparation and identification of the boundary and zone cell condition. Then, ANSYS Fluent simulator read the mesh and its properties. As temperature variations occur due to reaction kinetics, the energy equation is enabled in ANSYS Fluent to analyze the effect of temperature. The species transport model is enabled where reactions take place in bulk phase (volumetric reactions). The standard k-epsilon model is used to deal with turbulence. In order to deal with reactions, finite rate or eddy dissipation rate model is used where both rates are calculated and the minimum rate is considered. Reactions are enabled in the porous zone and are passed into the ANSYS Fluent by the user-defined database. Pressure drop is evaluated at different porosity levels, and the optimum value is attained. After pressure drop calculations, grid sensitivity analysis is performed. The model is validated by making a comparison between simulation pressure drop and Ergun equation pressure drop. Change in a mole fraction of species and exergy profile is evaluated. The sequential procedure starting from mesh generation to convergence of the solution is shown as given.

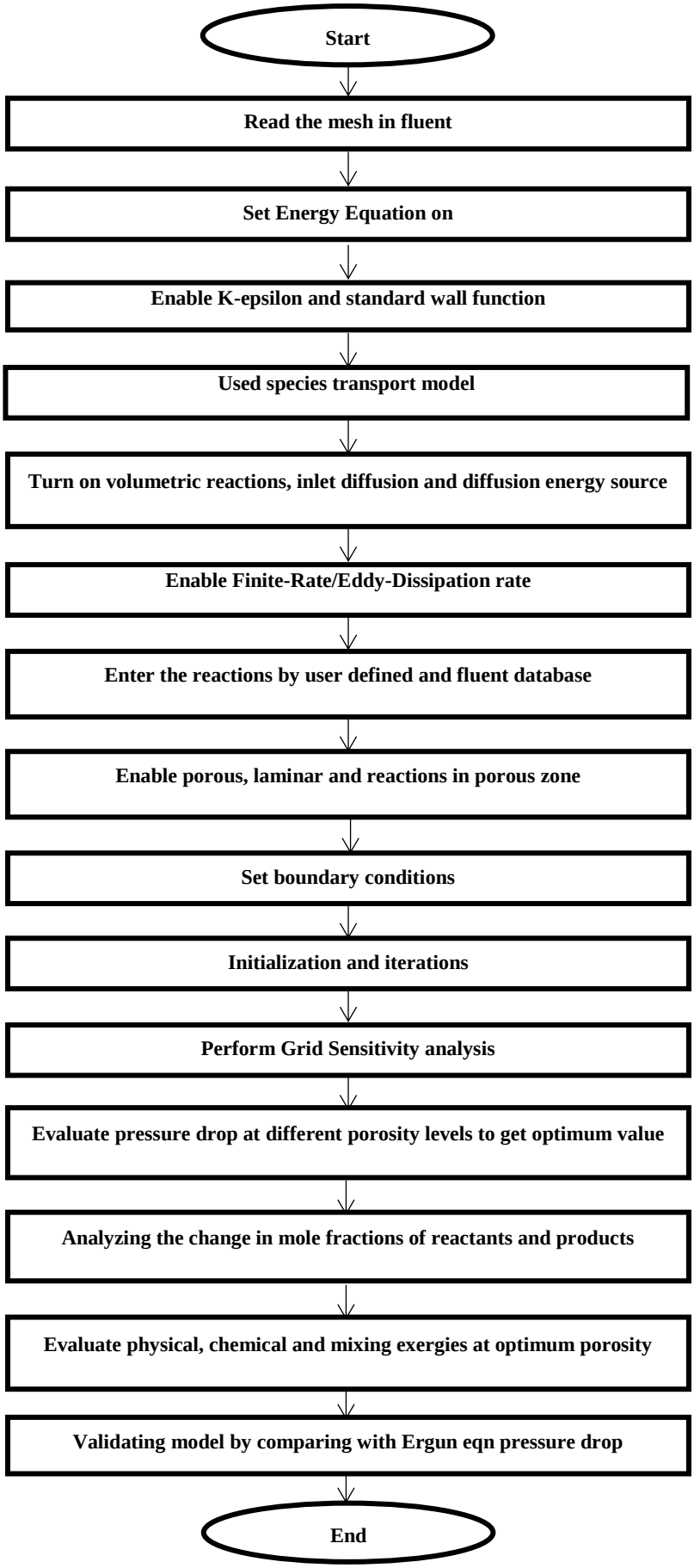

Figure 5.5: Schematic of Model Development Procedure

5.5 Grid Sensitivity analysis

An independent grid solution is achieved by the comparison of reactor 1 velocity profile with different meshes. Simulation is performed on four grids with 80000, 100000, 120000 and 125612 cells. The numerical uncertainty between grid cells 125612 and 120000 is less than 2 %. On the basis of this uncertainty level, mesh with cells 125612 is used.

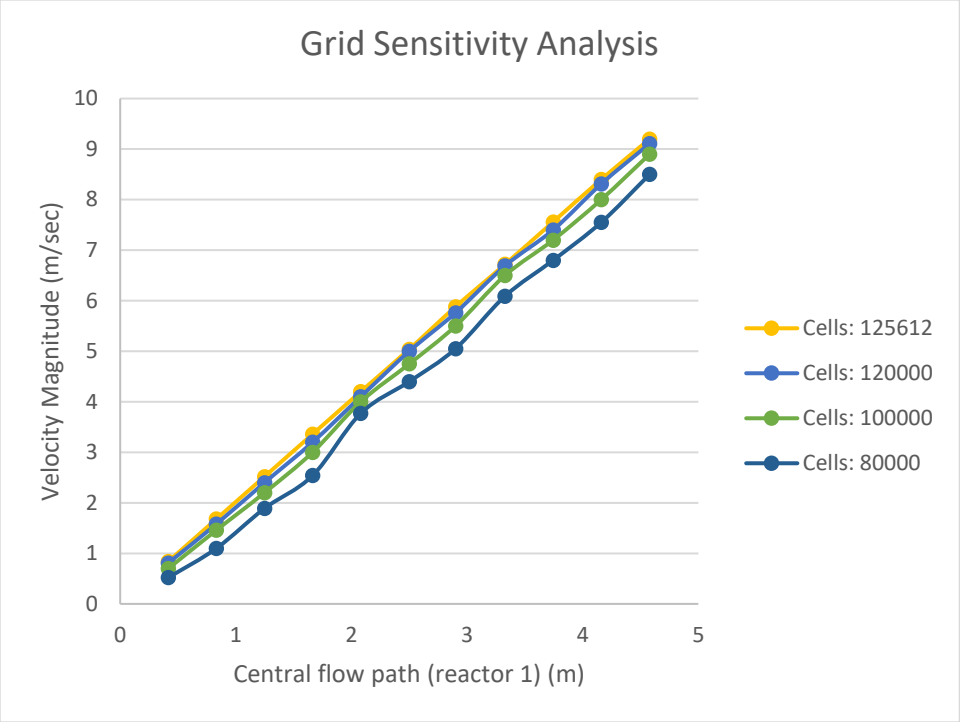

Figure 5.6: Grid Independent solution

Chapter-6

Results and Discussion

Physical, mixing and chemical exergies along with mole fraction of products and reactants are computed and discussed in this section. Table 6.2 demonstrates the physical exergetic efficiency of reactors. Table 6.3 indicates the values of mixing exergy. Percentage increase of chemical exergy in each reactor is shown in Table 6.4. Fig. 6.1-6.3 represents velocity, temperature, and pressure profile respectively. The mole fraction of n-heptane toluene, naphthene, iso-heptane and methane is shown in Fig. 6.4, 6.5, 6.6, 6.7 and 6.8, respectively. Fig. 6.9 and 6.10 shows variations of entropy and percentage turbulence intensity within system. The physical exergy and physical exergetic efficiency are illustrated in Fig. 6.11 and 6.12 respectively. Mixing, chemical, and total exergy are represented in Fig. 6.13, 6.14 and 6.15 respectively.

Table 6.1 shows the comparison of predicted pressure drop with the pressure drop obtained from Ergun equation at different porosity levels of bed 1, 2 and 3. Overall bed pressure drop decreases from reactor 1 to reactor 3. Average percentage error between the predicted value of pressure drop and pressure drop that is obtained from the Ergun equation is 5.38%, 5.03% and 4.8% in Bed 1, 2 and 3, respectively.

The irreversibilities generated in reactor 1 are greater than other two reactors due to the high pressure drop. This has caused a maximum decrease of physical exergetic efficiency in reactor 1 as shown in Table 6.2. In Table 6.3, it is observed that mixing phenomena decreases the exergy from reactor 1 to reactor 3. The decrease of exergy value in reactor 1, 2 and 3 is 128251.145 Joule/sec, 5700.04 Joule/sec and 1425.02 Joule/sec, respectively. Reactor 1 induces maximum mixing due to smaller size which results in considerable decrease of exergy value. The increased rate of reaction in reactor 1 produces species having high chemical potential. Hence the percentage increase of chemical exergy in reactor 1 is the greatest among three reactors. Table 6.4 shows the increase of chemical exergy from reactor 1 to reactor 3.

Fig. 6.1 shows the velocity profile of reactor 1, 2 and 3. In the annulus region, velocity increases sharply from around 6m/sec to 16m/sec due to decrease in the cross-sectional area. In fixed bed, a minimum velocity of 0.42 m/sec is achieved. As the fluid moves out from the fixed bed to the central pipe, its velocity again increases from 0.22m/sec to 8.4m/sec (approximately). Variation in flow area of three reactors ultimately affects the velocity profile. The maximum velocity in the central pipe of reactor 1, 2 and 3 is 8, 7.5 and 6.72m/sec, respectively.

Fig. 6.2 shows the temperature profile. Temperature decreases from 811K at the input of reactor 1 to 728K at the output of reactor 3. In reactor 1 dehydrogenation occurs which is a highly endothermic reaction and requires high temperature as an input. This causes a temperature drop of around 316K. In reactor 2, dehydrocyclization occurs which is less endothermic and has comparatively lower reaction rate thus causes less temperature drop (272K). In reactor 3, hydrocracking occurs which is an exothermic and having the slowest reaction rate. This causes a slight increase in temperature and results in a net temperature drop of around 5-8K. A similar trend of reactions is also observed by (Turaga and Ramanathan, 2003).

Fig. 6.3 shows the pressure profile at the porosity value of 0.3. The predicted pressure drop across reactor 1, 2 and 3 at porosity value of 0.3 is 5616.7, 6160.2 and 5979 Pascal respectively. In this case, pressure drop incorporate multiple effects like reaction rate, catalytic bed length, and height, annulus height, inlet mass flow rate, etc., hence an absolute trend is not obtained.

Fig. 6.4, 6.5, 6.6, 6.7 and 6.8 represent a change in a mole fraction of n-heptane, toluene, naphthene, iso-heptane and methane respectively. Mole fraction of n-heptane decreases from 0.55 to 0.275 through isomerization reaction while mole fraction of toluene increases up to 0.163 through dehydrocyclization reaction. Apart from naphthene, conversion of iso-heptane also takes place and their outlet mole fraction is 0.09 and 0.04, respectively. A slight increase in methane, ethane, propane, n-butane and n-pentane mole fraction is also observed as a result of hydrocracking reaction.

Physical exergy incorporates the mechanical and thermal exergies. Irreversible losses in the reactor are mainly due to viscous and inertial resistances which curtail the work potential in the reactor. Because of these resistances, a decrease in mechanical exergy is prominent as shown in Fig. 6.11. These losses can be overcome up to some extent by adjusting the permeability and inertial loss coefficient of fixed bed reactor to an optimum value. Most of the reactions of naphtha reforming are endothermic which cause a decrease in temperature and create irreversible losses. Therefore, a substantial decrease of physical exergetic efficiency along the length of the reactor is observed, Fig. 6.12. Initially, exergy of the feed components passing through the first reactor gradually decreases due to the irreversibilities caused by pressure drop, mixing and temperature drop. Exergy at the inlet of reactor 2 is equal to that of the outlet of reactor 1. Similarly, exergy at the inlet of reactor 3 is equal to that of the outlet of reactor 2. In Table 6.2, physical exergetic efficiency is calculated using equation 8. Fig. 6.12 shows the physical exergetic efficiency that is obtained by dividing the exergy values at each point to the input exergy value of the first reactor.

The mixing exergy always has a negative value as exergy of pure components is higher than the components in mixed form. Decrease in total exergy due to mixing is demonstrated in Fig. 6.13 (Bosmans et al., 2011). The exergy loss due to the mixing in reactor 1 is higher as compared to others. The high conversion rate in reactor 1 produces new product species at a faster rate that intensify the mixing effects. These effects create major irreversibilities and contribute significantly to the overall exergy destruction of naphtha reforming process. Within reactor 1, mixing effects are more prominent in the catalytic bed and approach constant value as gaseous products reach the central pipe.

Reactions generate products with higher chemical potential, so summation of chemical potential of products is higher than the reactants. Chemical exergy is increased from reactor 1 to reactor 3 as shown in Fig. 6.14. An average increase of chemical exergy of the three reactors is 0.177% (329353 joule/sec). In Fig. 6.15, the profile of total exergy is shown; which is the summation of physical, mixing and chemical exergies. The total exergy increases from 1.8813e+08 to 1.8868e+08 joule/sec. This increase in exergy

improves the total work potential of the system. The chemical exergy in all three reactors is increasing from the catalytic bed to the central pipe. The chemical reaction takes place in catalytic bed and produces new species. These species have high chemical potential and converge in the central pipe which ultimately increases the total chemical exergy. Because of slow reaction rate hydrocracking reaction takes place in the third reactor and releases heat due to its exothermic nature. This heat degrades the chemical energy of Naphthalene which results in loss of chemical exergy. This phenomenon causes slight increase of chemical exergy in the third reactor.

Table 6.1: Pressure drop at different porosities in Bed 1, Bed 2 and Bed 3

Porosity	$\left(\frac{\Delta P}{L}\right)_{1\ Pred}$	$\left(\frac{\Delta P}{L}\right)_{1\ Erg}$	% Error	$\left(\frac{\Delta P}{L}\right)_{2\ Pred}$	$\left(\frac{\Delta P}{L}\right)_{2\ Erg}$	% Error	$\left(\frac{\Delta P}{L}\right)_{3\ Pred}$	$\left(\frac{\Delta P}{L}\right)_{3\ Erg}$	% Error
0.1	6.83	6.5	5%	6.78	6.4	5.9%	4.9	4.7	4.2%
0.2	0.745	0.70	6%	0.73	0.70	4.2%	0.55	0.53	3.8%
0.3	0.1632	0.15	8.8%	0.16	0.152	5.2%	0.12	0.11	9%
0.4	0.0556	0.054	8%	0.0545	0.052	4.8%	0.0412	0.040	3%
0.5	0.0186	0.0180	3%	0.018	0.0172	4.6%	0.0137	0.0132	3.8%
0.6	0.0073	0.0070	4.2%	0.007	0.0067	4.5%	0.005	0.0047	6.4%
0.7	0.0021	0.0020	5%	0.0018	0.0017	5.9%	0.0016	0.00158	1.2%
0.8	0.00089	0.00084	6%	0.00074	0.00072	5.7%	0.00064	0.0006	6.7%
0.9	0.00082	0.00080	2.5%	0.00070	0.00067	4.5%	0.00061	0.00058	5.1%

Note: Pressure (psi) and Length (meter)

Table 6.2: Physical Exergetic Efficiency of Reactors

S.No	Physical Exergy In (Joule/Sec)	Physical Exergy Out (Joule/Sec)	Efficiency
Reactor 1	2427038.8	2108065.5	86.8%
Reactor 2	2108065.5	2073477.9	98.4%
Reactor 3	2073477.9	2058105.6	99.2%

Table 6.3: Effect of mixing on exergy values in Reactors

S.No	Mixing Exergy In (Joule/Sec)	Mixing Exergy Out (Joule/Sec)
Reactor 1	-98719.875	-226971.02
Reactor 2	-226971.02	-232671.06
Reactor 3	-232671.06	-234096.08

Table 6.4: Percentage increase of Chemical Exergy in Reactors

S.No	Chemical Exergy In (joule/sec)	Chemical Exergy Out (joule/sec)	% Increase of Chemical Exergy
Reactor 1	1.8579237e+08	1.8647971e+08	0.37%
Reactor 2	1.8652267e+08	1.8678043e+08	0.138%
Reactor 3	1.8678043e+08	1.8682339e+08	0.023%

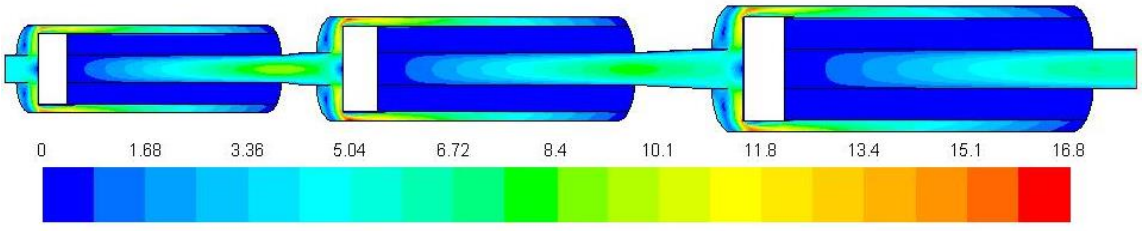

Figure 6.1: Velocity profile (m/sec)

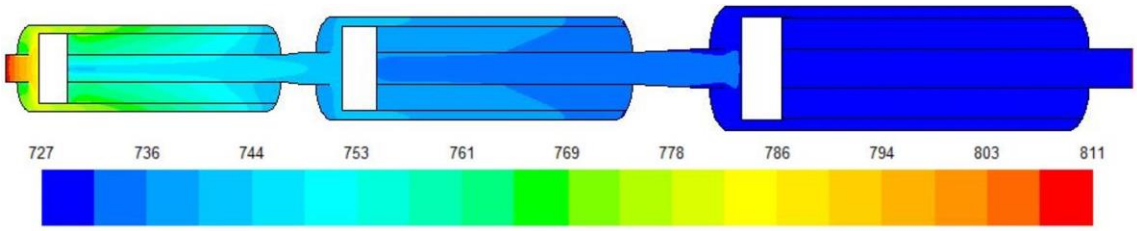

Figure 6.2: Temperature profile (K)

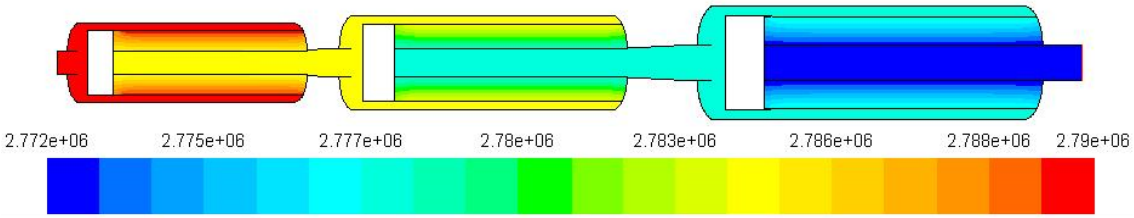

Figure 6.3: Pressure profile (Pascal)

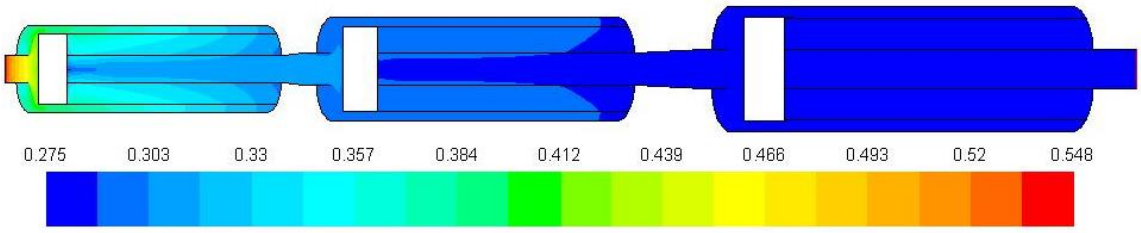

Figure 6.4: Mole fraction of n-heptane

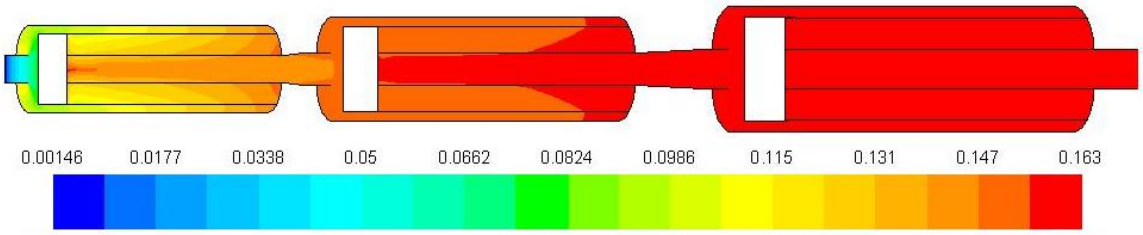

Figure 6.5: Mole fraction of toluene

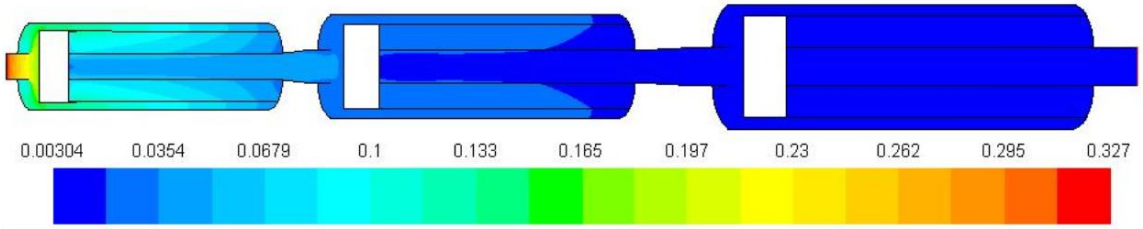

Figure 6.6: Mole fraction of naphthene

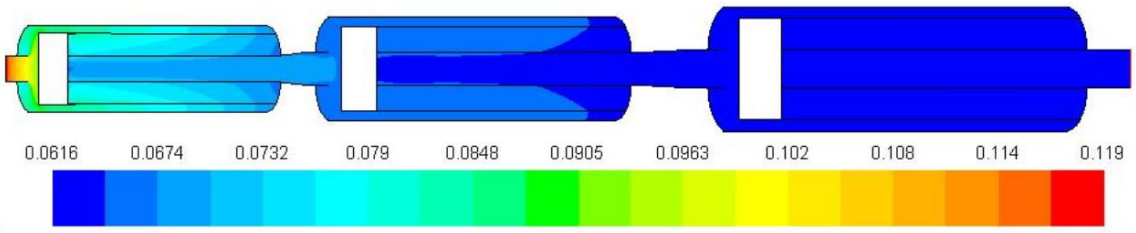

Figure 6.7: Mole fraction of iso-heptane

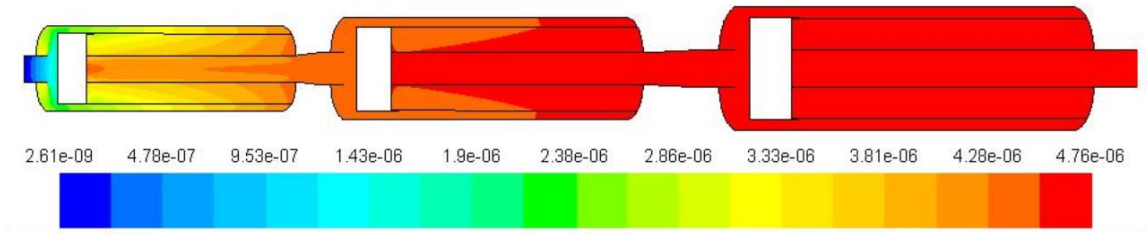

Figure 6.8: Mole fraction of methane

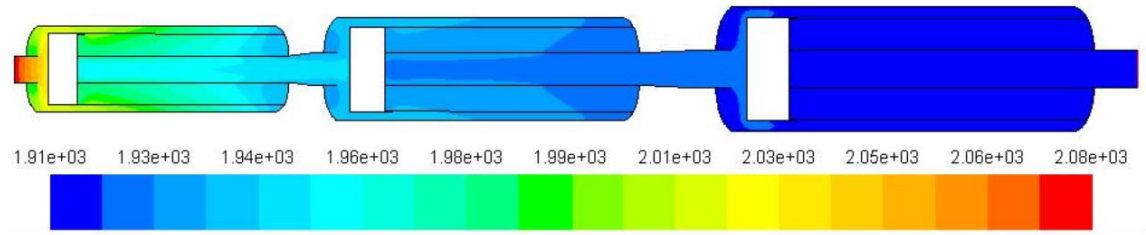

Figure 6.9: Contours of entropy (J/kg-K)

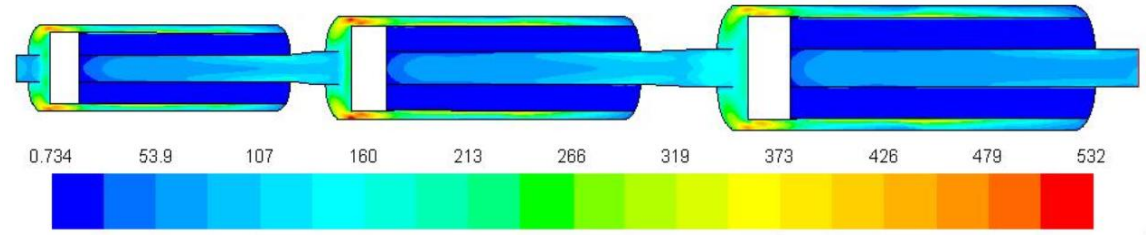

Figure 6.10: Turbulence intensity (%)

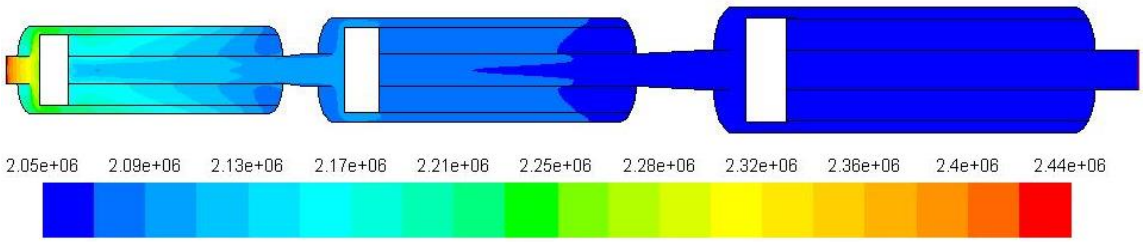

Figure 6.11: Physical Exergy (joule/sec)

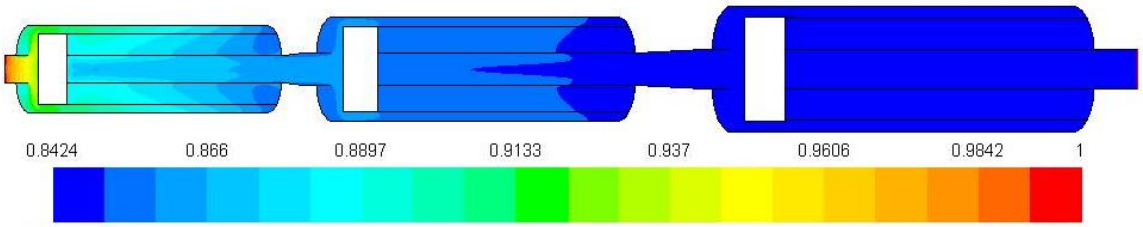

Figure 6.12: Physical exergetic efficiency

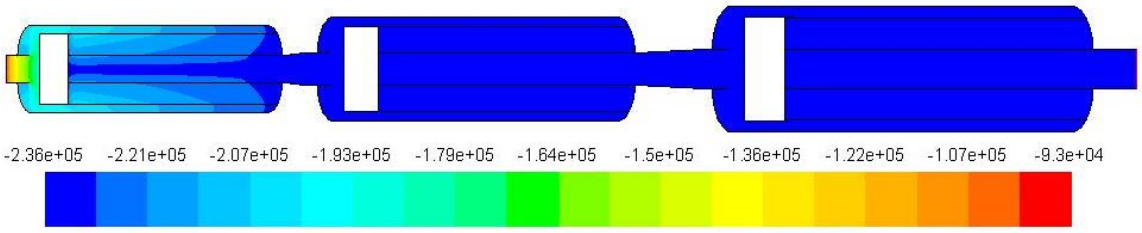

Figure 6.13: Mixing Exergy (joule/sec)

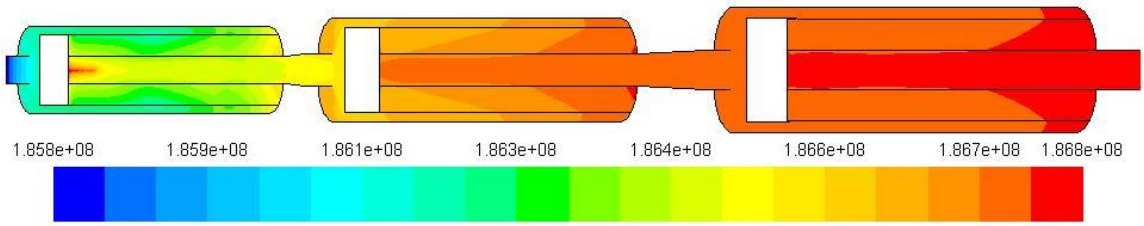

Figure 6.14: Chemical Exergy (joule/sec)

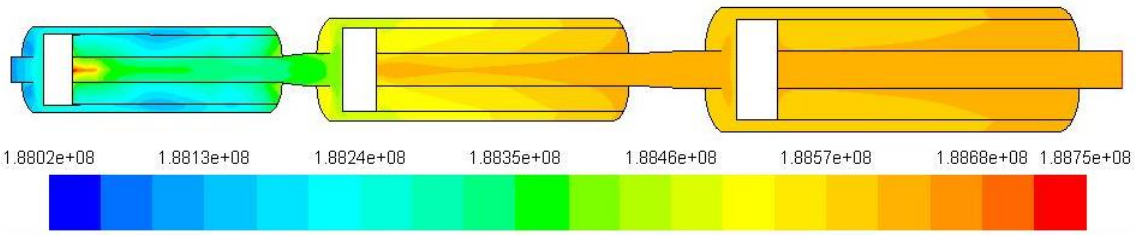

Figure 6.15: Total Exergy (joule/sec)

Chapter-7

Conclusions and Recommendations

In this study, a CFD model of naphtha reforming reactors is developed, and exergy analysis is performed. An interface is created with C language through an extension to incorporate reaction kinetics of naphtha reforming process. N-heptane fraction is used as a representative of the several hundred hydrocarbon components involved in the naphtha reforming reactions. The analysis involves the solution of the Navier-Stokes equations through SIMPLE algorithm and eddy viscosity is approximated using standard K-epsilon turbulence model. ANSYS Fluent is used to analyze the exergy variations in naphtha reforming reactors by identification of the required boundary and cell zone conditions in Gambit. Three reactors are used in the analysis of naphtha reforming process, and the results show that physical and mixing exergy decreases while chemical exergy increases from the first reactor to the third reactor due to the high chemical potential of the products.

In some refineries four reactors are used instead of three to improve performance. Further research can be undertaken to model four reactors and analyze their effects on the rate of reaction. Coking is a major problem in which carbon is deposited on the catalytic bed and can cause catalyst deactivation. Therefore, a detailed analysis of the effects of coking on exergy profile can be explored. As the ultimate goal of naphtha reforming process is to obtain gasoline with high Research Octane Number (RON). Hence examining the effect of exergetic efficiency on RON can be another research dimension for future work.

Appendix

Exergy codes

```
(custom-field-function/define
 '(((name pressure-exergy-joule-per-sec) (display "8.314 * 298 * ((c7h16<l> * 3937) / 100.21) * (
        ln ((molef-c7h16<l> * total-pressure) / 101325)) + 8.314 * 298 * ((ch3c6h11 * 3937) /
        98.186) * ( ln ((molef-ch3c6h11 * total-pressure) / 101325)) + 8.314 * 298 * ((c7h16 *
        3937) / 100.2) * ( ln ((molef-c7h16 * total-pressure) / 101325)) + 8.314 * 298 * ((h2 *
        3937) / 2) * ( ln ((molef-h2 * total-pressure) / 101325)) + 8.314 * 298 * ((c7h8 * 3937) /
        92) * ( ln ((molef-c7h8 * total-pressure) / 101325)) + 8.314 * 298 * ((ch4 * 3937) / 16) *
        ( ln ((molef-ch4 * total-pressure) / 101325)) + 8.314 * 298 * ((c2h6 * 3937) / 30) * ( ln
        ((molef-c2h6 * total-pressure) / 101325)) + 8.314 * 298 * ((c3h8 * 3937) / 44) * ( ln
        ((molef-c3h8 * total-pressure) / 101325)) + 8.314 * 298 * ((c4h10 * 3937) / 58) * ( ln
        ((molef-c4h10 * total-pressure) / 101325)) + 8.314 * 298 * ((c5h12 * 3937) / 72) * ( ln
        ((molef-c5h12 * total-pressure) / 101325))") (syntax-tree ("+" ("+" ("+" ("+" ("+" ("+" ("+"
        ("+" ("+" ("*" ("*" 2477.572 ("/" ("*" "c7h16<l>" 3937) 100.21)) ("log" ("/" ("*" "molef-
        c7h16<l>" "total-pressure") 101325))) ("*" ("*" 2477.572 ("/" ("*" "ch3c6h11" 3937)
        98.18600000000001)) ("log" ("/" ("*" "molef-ch3c6h11" "total-pressure") 101325))))
        ("*" ("*" 2477.572 ("/" ("*" "c7h16" 3937) 100.2)) ("log" ("/" ("*" "molef-c7h16" "total-
        pressure") 101325)))) ("*" ("*" 2477.572 ("/" ("*" "h2" 3937) 2)) ("log" ("/" ("*" "molef-
        h2" "total-pressure") 101325)))) ("*" ("*" 2477.572 ("/" ("*" "c7h8" 3937) 92)) ("log" ("/"
        ("*" "molef-c7h8" "total-pressure") 101325)))) ("*" ("*" 2477.572 ("/" ("*" "ch4" 3937)
        16)) ("log" ("/" ("*" "molef-ch4" "total-pressure") 101325)))) ("*" ("*" 2477.572 ("/" ("*"
        "c2h6" 3937) 30)) ("log" ("/" ("*" "molef-c2h6" "total-pressure") 101325)))) ("*" ("*"
        2477.572 ("/" ("*" "c3h8" 3937) 44)) ("log" ("/" ("*" "molef-c3h8" "total-pressure")
        101325)))) ("*" ("*" 2477.572 ("/" ("*" "c4h10" 3937) 58)) ("log" ("/" ("*" "molef-c4h10"
        "total-pressure") 101325)))) ("*" ("*" 2477.572 ("/" ("*" "c5h12" 3937) 72)) ("log" ("/"
        ("*" "molef-c5h12" "total-pressure") 101325))))) (code (field-+ (field-+ (field-+ (field-+
        (field-+ (field-+ (field-+ (field-+ (field-+ (field-* (field-* 2477.572 (field-/ (field-* (field-load
        "c7h16<l>") 3937) 100.21)) (field-log (field-/ (field-* (field-load "molef-c7h16<l>") (field-
        load "total-pressure")) 101325))) (field-* (field-* 2477.572 (field-/ (field-* (field-load
        "ch3c6h11") 3937) 98.18600000000001)) (field-log (field-/ (field-* (field-load "molef-
        ch3c6h11") (field-load "total-pressure")) 101325)))) (field-* (field-* 2477.572 (field-/
        (field-* (field-load "c7h16") 3937) 100.2)) (field-log (field-/ (field-* (field-load "molef-
        c7h16") (field-load "total-pressure")) 101325)))) (field-* (field-* 2477.572 (field-/ (field-
        * (field-load "h2") 3937) 2)) (field-log (field-/ (field-* (field-load "molef-h2") (field-load
        "total-pressure")) 101325)))) (field-* (field-* 2477.572 (field-/ (field-* (field-load "c7h8")
        3937) 92)) (field-log (field-/ (field-* (field-load "molef-c7h8") (field-load "total-
        pressure")) 101325)))) (field-* (field-* 2477.572 (field-/ (field-* (field-load "ch4") 3937)
        16)) (field-log (field-/ (field-* (field-load "molef-ch4") (field-load "total-pressure"))
        101325)))) (field-* (field-* 2477.572 (field-/ (field-* (field-load "c2h6") 3937) 30)) (field-
        log (field-/ (field-* (field-load "molef-c2h6") (field-load "total-pressure")) 101325))))
        (field-* (field-* 2477.572 (field-/ (field-* (field-load "c3h8") 3937) 44)) (field-log (field-/
        (field-* (field-load "molef-c3h8") (field-load "total-pressure")) 101325)))) (field-* (field-*
        2477.572 (field-/ (field-* (field-load "c4h10") 3937) 58)) (field-log (field-/ (field-* (field-
        load "molef-c4h10") (field-load "total-pressure")) 101325)))) (field-* (field-* 2477.572
```

(field-/ (field-* (field-load "c5h12") 3937) 72)) (field-log (field-/ (field-* (field-load "molef-c5h12") (field-load "total-pressure")) 101325))))))
((name a) (display "temperature - 298") (syntax-tree ("-" "temperature" 298)) (code (field-- (field-load "temperature") 298)))
((name b) (display "temperature * temperature - 298 * 298") (syntax-tree ("-" ("*" "temperature" "temperature") 88804)) (code (field-- (field-* (field-load "temperature") (field-load "temperature")) 88804)))
((name c) (display "temperature * temperature * temperature - 298 * 298 * 298") (syntax-tree ("-" ("*" ("*" "temperature" "temperature") "temperature") 26463592)) (code (field-- (field-* (field-* (field-load "temperature") (field-load "temperature")) (field-load "temperature")) 26463592)))
((name d) (display "temperature * temperature * temperature * temperature - 298 * 298 * 298 * 298") (syntax-tree ("-" ("*" ("*" ("*" "temperature" "temperature") "temperature") "temperature") -703784176)) (code (field-- (field-* (field-* (field-* (field-load "temperature") (field-load "temperature")) (field-load "temperature")) (field-load "temperature")) -703784176)))
((name e) (display "temperature - 298 - 298 * ln (temperature / 298)") (syntax-tree ("-" ("-" "temperature" 298) ("*" 298 ("log" ("/" "temperature" 298))))) (code (field-- (field-- (field-load "temperature") 298) (field-* 298 (field-log (field-/ (field-load "temperature") 298))))))
((name t1) (display "(((c7h16<l> * 3937) / 100.21) * ((- 5.146 * (a) + (.6762 / 2) * (b) + (- .0003651 / 3) * (c) + (.00000007658 / 4) * (d)) / (a)) * (e))") (syntax-tree ("*" ("*" ("/" ("*" "c7h16<l>" 3937) 100.21) ("/" ("+" ("+" ("+" ("*" -5.146 "a") ("*" 0.3381 "b")) ("*" -0.0001217 "c")) ("*" 1.9145e-08 "d")) "a")) "e")) (code (field-* (field-* (field-/ (field-* (field-load "c7h16<l>") 3937) 100.21) (field-/ (field-+ (field-+ (field-+ (field-* -5.146 (cx-field-eval "a")) (field-* 0.3381 (cx-field-eval "b"))) (field-* -0.0001217 (cx-field-eval "c"))) (field-* 1.9145e-08 (cx-field-eval "d"))) (cx-field-eval "a"))) (cx-field-eval "e"))))
((name t2) (display "(((ch3c6h11 * 3937) / 98.186) * ((- 61.92 * (a) + (.7842 / 2) * (b) + (- .0004438 / 3) * (c) + (.00000009366 / 4) * (d)) / (a)) * (e))") (syntax-tree ("*" ("*" ("/" ("*" "ch3c6h11" 3937) 98.18600000000001) ("/" ("+" ("+" ("+" ("*" -61.92 "a") ("*" 0.3921 "b")) ("*" -0.0001479333333333333 "c")) ("*" 2.3415e-08 "d")) "a")) "e")) (code (field-* (field-* (field-/ (field-* (field-load "ch3c6h11") 3937) 98.18600000000001) (field-/ (field-+ (field-+ (field-+ (field-* -61.92 (cx-field-eval "a")) (field-* 0.3921 (cx-field-eval "b"))) (field-* -0.0001479333333333333 (cx-field-eval "c"))) (field-* 2.3415e-08 (cx-field-eval "d"))) (cx-field-eval "a"))) (cx-field-eval "e"))))
((name t3) (display "(((c7h16 * 3937) / 100.2) * ((- 39.39 * (a) + (.8642 / 2) * (b) + (- .0006289 / 3) * (c) + (.0000001836 / 4) * (d)) / (a)) * (e))") (syntax-tree ("*" ("*" ("/" ("*" "c7h16" 3937) 100.2) ("/" ("+" ("+" ("+" ("*" -39.39 "a") ("*" 0.4321 "b")) ("*" -0.0002096333333333334 "c")) ("*" 4.59e-08 "d")) "a")) "e")) (code (field-* (field-* (field-/ (field-* (field-load "c7h16") 3937) 100.2) (field-/ (field-+ (field-+ (field-+ (field-* -39.39 (cx-field-eval "a")) (field-* 0.4321 (cx-field-eval "b"))) (field-* -0.0002096333333333334 (cx-field-eval "c"))) (field-* 4.59e-08 (cx-field-eval "d"))) (cx-field-eval "a"))) (cx-field-eval "e"))))
((name t4) (display "(((h2 * 3937) / 2) * ((27.14 * (a) + (.009274 / 2) * (b) + (- .00001381 / 3) * (c) + (.000000008654 / 4) * (d)) / (a)) * (e))") (syntax-tree ("*" ("*" ("/" ("*" "h2" 3937) 2) ("/" ("+" ("+" ("+" ("*" 27.14 "a") ("*" 0.004637 "b")) ("*" -4.603333333333333e-06 "c")) ("*" 2.1635e-09 "d")) "a")) "e")) (code (field-* (field-* (field-/ (field-* (field-load "h2") 3937) 2) (field-/ (field-+ (field-+ (field-+ (field-* 27.14 (cx-field-eval "a")) (field-* 0.004637

(cx-field-eval "b"))) (field-* -4.603333333333333e-06 (cx-field-eval "c"))) (field-* 2.1635e-09 (cx-field-eval "d"))) (cx-field-eval "a"))) (cx-field-eval "e"))))
((name t5) (display "(((c7h8 * 3937) / 92) * ((- 24.35 * (a) + (.5125 / 2) * (b) + (- .0002765 / 3) * (c) + (.00000004911 / 4) * (d)) / (a)) * (e))") (syntax-tree ("*" ("*" ("/" ("*" "c7h8" 3937) 92) ("/" ("+" ("+" ("+" ("*" -24.35 "a") ("*" 0.25625 "b")) ("*" -9.216666666666667e-05 "c")) ("*" 1.22775e-08 "d")) "a")) "e")) (code (field-* (field-* (field-/ (field-* (field-load "c7h8") 3937) 92) (field-/ (field-+ (field-+ (field-+ (field-* -24.35 (cx-field-eval "a")) (field-* 0.25625 (cx-field-eval "b"))) (field-* -9.216666666666667e-05 (cx-field-eval "c"))) (field-* 1.22775e-08 (cx-field-eval "d"))) (cx-field-eval "a"))) (cx-field-eval "e"))))
((name t6) (display "(((ch4 * 3937) / 16) * ((19.25 * (a) + (.05213 / 2) * (b) + (.00001197 / 3) * (c) + (- .00000001132 / 4) * (d)) / (a)) * (e))") (syntax-tree ("*" ("*" ("/" ("*" "ch4" 3937) 16) ("/" ("+" ("+" ("+" ("*" 19.25 "a") ("*" 0.026065 "b")) ("*" 3.99e-06 "c")) ("*" -2.83e-09 "d")) "a")) "e")) (code (field-* (field-* (field-/ (field-* (field-load "ch4") 3937) 16) (field-/ (field-+ (field-+ (field-+ (field-* 19.25 (cx-field-eval "a")) (field-* 0.026065 (cx-field-eval "b"))) (field-* 3.99e-06 (cx-field-eval "c"))) (field-* -2.83e-09 (cx-field-eval "d"))) (cx-field-eval "a"))) (cx-field-eval "e"))))
((name t7) (display "(((c2h6 * 3937) / 30) * ((5.409 * (a) + (.1781 / 2) * (b) + (- .00006938 / 3) * (c) + (.000000008713 / 4) * (d)) / (a)) * (e))") (syntax-tree ("*" ("*" ("/" ("*" "c2h6" 3937) 30) ("/" ("+" ("+" ("+" ("*" 5.409 "a") ("*" 0.08905 "b")) ("*" -2.312666666666667e-05 "c")) ("*" 2.17825e-09 "d")) "a")) "e")) (code (field-* (field-* (field-/ (field-* (field-load "c2h6") 3937) 30) (field-/ (field-+ (field-+ (field-+ (field-* 5.409 (cx-field-eval "a")) (field-* 0.08905 (cx-field-eval "b"))) (field-* -2.312666666666667e-05 (cx-field-eval "c"))) (field-* 2.17825e-09 (cx-field-eval "d"))) (cx-field-eval "a"))) (cx-field-eval "e"))))
((name t8) (display "(((c3h8 * 3937) / 44) * ((- 4.224 * (a) + (.3063 / 2) * (b) + (- .0001586 / 3) * (c) + (.00000003215 / 4) * (d)) / (a)) * (e))") (syntax-tree ("*" ("*" ("/" ("*" "c3h8" 3937) 44) ("/" ("+" ("+" ("+" ("*" -4.224 "a") ("*" 0.15315 "b")) ("*" -5.286666666666667e-05 "c")) ("*" 8.0375e-09 "d")) "a")) "e")) (code (field-* (field-* (field-/ (field-* (field-load "c3h8") 3937) 44) (field-/ (field-+ (field-+ (field-+ (field-* -4.224 (cx-field-eval "a")) (field-* 0.15315 (cx-field-eval "b"))) (field-* -5.286666666666667e-05 (cx-field-eval "c"))) (field-* 8.0375e-09 (cx-field-eval "d"))) (cx-field-eval "a"))) (cx-field-eval "e"))))
((name t9) (display "(((c4h10 * 3937) / 58) * ((9.487 * (a) + (.3313 / 2) * (b) + (- .0001108 / 3) * (c) + (- .000000002822 / 4) * (d)) / (a)) * (e))") (syntax-tree ("*" ("*" ("/" ("*" "c4h10" 3937) 58) ("/" ("+" ("+" ("+" ("*" 9.487 "a") ("*" 0.16565 "b")) ("*" -3.693333333333333e-05 "c")) ("*" -7.055e-10 "d")) "a")) "e")) (code (field-* (field-* (field-/ (field-* (field-load "c4h10") 3937) 58) (field-/ (field-+ (field-+ (field-+ (field-* 9.487 (cx-field-eval "a")) (field-* 0.16565 (cx-field-eval "b"))) (field-* -3.693333333333333e-05 (cx-field-eval "c"))) (field-* -7.055e-10 (cx-field-eval "d"))) (cx-field-eval "a"))) (cx-field-eval "e"))))
((name t10) (display "(((c5h12 * 3937) / 72) * ((- 3.262 * (a) + (.4893 / 2) * (b) + (- .0002580 / 3) * (c) + (.00000005305 / 4) * (d)) / (a)) * (e))") (syntax-tree ("*" ("*" ("/" ("*" "c5h12" 3937) 72) ("/" ("+" ("+" ("+" ("*" -3.262 "a") ("*" 0.24465 "b")) ("*" -8.599999999999999e-05 "c")) ("*" 1.32625e-08 "d")) "a")) "e")) (code (field-* (field-* (field-/ (field-* (field-load "c5h12") 3937) 72) (field-/ (field-+ (field-+ (field-+ (field-* -3.262 (cx-field-eval "a")) (field-* 0.24465 (cx-field-eval "b"))) (field-* -8.599999999999999e-05 (cx-field-eval "c"))) (field-* 1.32625e-08 (cx-field-eval "d"))) (cx-field-eval "a"))) (cx-field-eval "e"))))
((name thermal-exergy-joule-per-sec) (display "t1 + t2 + t3 + t4 + t5 + t6 + t7 + t8 + t9 + t10") (syntax-tree ("+" ("+" ("+" ("+" ("+" ("+" ("+" ("+" ("+" "t1" "t2") "t3") "t4") "t5") "t6") "t7") "t8") "t9") "t10")) (code (field-+ (field-+ (field-+ (field-+ (field-+ (field-+ (field-+ (field-+

(field-+ (cx-field-eval "t1") (cx-field-eval "t2")) (cx-field-eval "t3")) (cx-field-eval "t4")) (cx-field-eval "t5")) (cx-field-eval "t6")) (cx-field-eval "t7")) (cx-field-eval "t8")) (cx-field-eval "t9")) (cx-field-eval "t10"))))

((name f) (display "((ch3c6h11 * 3937) / 98.186) + ((c7h16<l> * 3937) / 100.21) + ((c7h16 * 3937) / 100.2) + ((h2 * 3937) / 2) + ((c7h8 * 3937) / 92) + ((ch4 * 3937) / 16) + ((c2h6 * 3937) / 30) + ((c3h8 * 3937) / 44) + ((c4h10 * 3937) / 58) + ((c5h12 * 3937) / 72)") (syntax-tree ("+" ("+" ("+" ("+" ("+" ("+" ("+" ("+" ("+" ("/" ("*" "ch3c6h11" 3937) 98.18600000000001) ("/" ("*" "c7h16<l>" 3937) 100.21)) ("/" ("*" "c7h16" 3937) 100.2)) ("/" ("*" "h2" 3937) 2)) ("/" ("*" "c7h8" 3937) 92)) ("/" ("*" "ch4" 3937) 16)) ("/" ("*" "c2h6" 3937) 30)) ("/" ("*" "c3h8" 3937) 44)) ("/" ("*" "c4h10" 3937) 58)) ("/" ("*" "c5h12" 3937) 72))) (code (field-+ (field-+ (field-+ (field-+ (field-+ (field-+ (field-+ (field-+ (field-+ (field-/ (field-* (field-load "ch3c6h11") 3937) 98.18600000000001) (field-/ (field-* (field-load "c7h16<l>") 3937) 100.21)) (field-/ (field-* (field-load "c7h16") 3937) 100.2)) (field-/ (field-* (field-load "h2") 3937) 2)) (field-/ (field-* (field-load "c7h8") 3937) 92)) (field-/ (field-* (field-load "ch4") 3937) 16)) (field-/ (field-* (field-load "c2h6") 3937) 30)) (field-/ (field-* (field-load "c3h8") 3937) 44)) (field-/ (field-* (field-load "c4h10") 3937) 58)) (field-/ (field-* (field-load "c5h12") 3937) 72))))

((name m1) (display "8.314 * 298 * ((c7h16<l> * 3937) / 100.21) * ln (((c7h16<l> * 3937) / 100.21) / (f))") (syntax-tree ("*" ("*" 2477.572 ("/" ("*" "c7h16<l>" 3937) 100.21)) ("log" ("/" ("/" ("*" "c7h16<l>" 3937) 100.21) "f")))) (code (field-* (field-* 2477.572 (field-/ (field-* (field-load "c7h16<l>") 3937) 100.21)) (field-log (field-/ (field-/ (field-* (field-load "c7h16<l>") 3937) 100.21) (cx-field-eval "f"))))))

((name m2) (display "8.314 * 298 * ((ch3c6h11 * 3937) / 98.186) * ln (((ch3c6h11 * 3937) / 98.186) / (f))") (syntax-tree ("*" ("*" 2477.572 ("/" ("*" "ch3c6h11" 3937) 98.18600000000001)) ("log" ("/" ("/" ("*" "ch3c6h11" 3937) 98.18600000000001) "f")))) (code (field-* (field-* 2477.572 (field-/ (field-* (field-load "ch3c6h11") 3937) 98.18600000000001)) (field-log (field-/ (field-/ (field-* (field-load "ch3c6h11") 3937) 98.18600000000001) (cx-field-eval "f"))))))

((name m3) (display "8.314 * 298 * ((c7h16 * 3937) / 100.2) * ln (((c7h16 * 3937) / 100.2) / (f))") (syntax-tree ("*" ("*" 2477.572 ("/" ("*" "c7h16" 3937) 100.2)) ("log" ("/" ("/" ("*" "c7h16" 3937) 100.2) "f")))) (code (field-* (field-* 2477.572 (field-/ (field-* (field-load "c7h16") 3937) 100.2)) (field-log (field-/ (field-/ (field-* (field-load "c7h16") 3937) 100.2) (cx-field-eval "f"))))))

((name m4) (display "8.314 * 298 * ((h2 * 3937) / 2) * ln (((h2 * 3937) / 2) / (f))") (syntax-tree ("*" ("*" 2477.572 ("/" ("*" "h2" 3937) 2)) ("log" ("/" ("/" ("*" "h2" 3937) 2) "f")))) (code (field-* (field-* 2477.572 (field-/ (field-* (field-load "h2") 3937) 2)) (field-log (field-/ (field-/ (field-* (field-load "h2") 3937) 2) (cx-field-eval "f"))))))

((name m5) (display "8.314 * 298 * ((c7h8 * 3937) / 92) * ln (((c7h8 * 3937) / 92) / (f))") (syntax-tree ("*" ("*" 2477.572 ("/" ("*" "c7h8" 3937) 92)) ("log" ("/" ("/" ("*" "c7h8" 3937) 92) "f")))) (code (field-* (field-* 2477.572 (field-/ (field-* (field-load "c7h8") 3937) 92)) (field-log (field-/ (field-/ (field-* (field-load "c7h8") 3937) 92) (cx-field-eval "f"))))))

((name m6) (display "8.314 * 298 * ((ch4 * 3937) / 16) * ln (((ch4 * 3937) / 16) / (f))") (syntax-tree ("*" ("*" 2477.572 ("/" ("*" "ch4" 3937) 16)) ("log" ("/" ("/" ("*" "ch4" 3937) 16) "f")))) (code (field-* (field-* 2477.572 (field-/ (field-* (field-load "ch4") 3937) 16)) (field-log (field-/ (field-/ (field-* (field-load "ch4") 3937) 16) (cx-field-eval "f"))))))

((name m7) (display "8.314 * 298 * ((c2h6 * 3937) / 30) * ln (((c2h6 * 3937) / 30) / (f))") (syntax-tree ("*" ("*" 2477.572 ("/" ("*" "c2h6" 3937) 30)) ("log" ("/" ("/" ("*" "c2h6" 3937) 30)

"f")))) (code (field-* (field-* 2477.572 (field-/ (field-* (field-load "c2h6") 3937) 30)) (field-log (field-/ (field-/ (field-* (field-load "c2h6") 3937) 30) (cx-field-eval "f"))))))
((name m8) (display "8.314 * 298 * ((c3h8 * 3937) / 44) * ln (((c3h8 * 3937) / 44) / (f))") (syntax-tree ("*" ("*" 2477.572 ("/" ("*" "c3h8" 3937) 44)) ("log" ("/" ("/" ("*" "c3h8" 3937) 44) "f")))) (code (field-* (field-* 2477.572 (field-/ (field-* (field-load "c3h8") 3937) 44)) (field-log (field-/ (field-/ (field-* (field-load "c3h8") 3937) 44) (cx-field-eval "f"))))))
((name m9) (display "8.314 * 298 * ((c4h10 * 3937) / 58) * ln (((c4h10 * 3937) / 58) / (f))") (syntax-tree ("*" ("*" 2477.572 ("/" ("*" "c4h10" 3937) 58)) ("log" ("/" ("/" ("*" "c4h10" 3937) 58) "f")))) (code (field-* (field-* 2477.572 (field-/ (field-* (field-load "c4h10") 3937) 58)) (field-log (field-/ (field-/ (field-* (field-load "c4h10") 3937) 58) (cx-field-eval "f"))))))
((name m10) (display "8.314 * 298 * ((c5h12 * 3937) / 72) * ln (((c5h12 * 3937) / 72) / (f))") (syntax-tree ("*" ("*" 2477.572 ("/" ("*" "c5h12" 3937) 72)) ("log" ("/" ("/" ("*" "c5h12" 3937) 72) "f")))) (code (field-* (field-* 2477.572 (field-/ (field-* (field-load "c5h12") 3937) 72)) (field-log (field-/ (field-/ (field-* (field-load "c5h12") 3937) 72) (cx-field-eval "f"))))))
((name mixing-exergy-joule-per-sec) (display "m1 + m2 + m3 + m4 + m5 + m6 + m7 + m8 + m9 + m10") (syntax-tree ("+" ("+" ("+" ("+" ("+" ("+" ("+" ("+" ("+" "m1" "m2") "m3") "m4") "m5") "m6") "m7") "m8") "m9") "m10")) (code (field-+ (field-+ (field-+ (field-+ (field-+ (field-+ (field-+ (field-+ (field-+ (cx-field-eval "m1") (cx-field-eval "m2")) (cx-field-eval "m3")) (cx-field-eval "m4")) (cx-field-eval "m5")) (cx-field-eval "m6")) (cx-field-eval "m7")) (cx-field-eval "m8")) (cx-field-eval "m9")) (cx-field-eval "m10"))))
((name c1) (display "((c7h16<l> * 3937) / 100.21) * 4769294.56") (syntax-tree ("*" ("/" ("*" "c7h16<l>" 3937) 100.21) 4769294.56)) (code (field-* (field-/ (field-* (field-load "c7h16<l>") 3937) 100.21) 4769294.56)))
((name c2) (display "((ch3c6h11 * 3937) / 98.186) * 4551729.68") (syntax-tree ("*" ("/" ("*" "ch3c6h11" 3937) 98.18600000000001) 4551729.68)) (code (field-* (field-/ (field-* (field-load "ch3c6h11") 3937) 98.18600000000001) 4551729.68)))
((name c3) (display "((c7h16 * 3937) / 100.2) * 4764650.32") (syntax-tree ("*" ("/" ("*" "c7h16" 3937) 100.2) 4764650.32)) (code (field-* (field-/ (field-* (field-load "c7h16") 3937) 100.2) 4764650.32)))
((name c4) (display "((h2 * 3937) / 2) * 236100") (syntax-tree ("*" ("/" ("*" "h2" 3937) 2) 236100)) (code (field-* (field-/ (field-* (field-load "h2") 3937) 2) 236100)))
((name c5) (display "((c7h8 * 3937) / 92) * 3938439.952") (syntax-tree ("*" ("/" ("*" "c7h8" 3937) 92) 3938439.952)) (code (field-* (field-/ (field-* (field-load "c7h8") 3937) 92) 3938439.952)))
((name c6) (display "((ch4 * 3937) / 16) * 831656.24") (syntax-tree ("*" ("/" ("*" "ch4" 3937) 16) 831656.24)) (code (field-* (field-/ (field-* (field-load "ch4") 3937) 16) 831656.24)))
((name c7) (display "((c2h6 * 3937) / 30) * 1495913.76") (syntax-tree ("*" ("/" ("*" "c2h6" 3937) 30) 1495913.76)) (code (field-* (field-/ (field-* (field-load "c2h6") 3937) 30) 1495913.76)))
((name c8) (display "((c3h8 * 3937) / 44) * 2151661.024") (syntax-tree ("*" ("/" ("*" "c3h8" 3937) 44) 2151661.024)) (code (field-* (field-/ (field-* (field-load "c3h8") 3937) 44) 2151661.024)))
((name c9) (display "((c4h10 * 3937) / 58) * 2805793.264") (syntax-tree ("*" ("/" ("*" "c4h10" 3937) 58) 2805793.264)) (code (field-* (field-/ (field-* (field-load "c4h10") 3937) 58) 2805793.264)))
((name c10) (display "((c5h12 * 3937) / 72) * 3459649.36") (syntax-tree ("*" ("/" ("*" "c5h12" 3937) 72) 3459649.36)) (code (field-* (field-/ (field-* (field-load "c5h12") 3937) 72) 3459649.36)))

((name chemical-exergy-joule-per-sec) (display "c1 + c2 + c3 + c4 + c5 + c6 + c7 + c8 + c9 + c10") (syntax-tree ("+" ("+" ("+" ("+" ("+" ("+" ("+" ("+" ("+" "c1" "c2") "c3") "c4") "c5") "c6") "c7") "c8") "c9") "c10")) (code (field-+ (field-+ (field-+ (field-+ (field-+ (field-+ (field-+ (field-+ (field-+ (cx-field-eval "c1") (cx-field-eval "c2")) (cx-field-eval "c3")) (cx-field-eval "c4")) (cx-field-eval "c5")) (cx-field-eval "c6")) (cx-field-eval "c7")) (cx-field-eval "c8")) (cx-field-eval "c9")) (cx-field-eval "c10"))))
((name total-exergy-joule-per-sec) (display "pressure-exergy-joule-per-sec + thermal-exergy-joule-per-sec + mixing-exergy-joule-per-sec + chemical-exergy-joule-per-sec") (syntax-tree ("+" ("+" ("+" "pressure-exergy-joule-per-sec" "thermal-exergy-joule-per-sec") "mixing-exergy-joule-per-sec") "chemical-exergy-joule-per-sec")) (code (field-+ (field-+ (field-+ (cx-field-eval "pressure-exergy-joule-per-sec") (cx-field-eval "thermal-exergy-joule-per-sec")) (cx-field-eval "mixing-exergy-joule-per-sec")) (cx-field-eval "chemical-exergy-joule-per-sec"))))

References

[1] G. Tverberg. *BP Data Suggests We Are Reaching Peak Energy Demand*. Available: https://ourfiniteworld.com/2015/06/23/bp-data-suggests-we-are-reaching-peak-energy-demand/

[2] I. E. Agency, "IEA finds CO2 emissions flat for third straight year even as global economy grew in 2016," 2017, March 17.

[3] A. Hinderink, F. Kerkhof, A. Lie, J. D. S. Arons, and H. Van Der Kooi, "Exergy analysis with a flowsheeting simulator—I. Theory; calculating exergies of material streams," *Chemical Engineering Science,* vol. 51, pp. 4693-4700, 1996.

[4] S. de Oliveira, "Exergy, exergy costing, and renewability analysis of energy conversion processes," in *Exergy*, ed: Springer, 2013, pp. 5-53.

[5] M. A. Rosen, I. Dincer, and M. Kanoglu, "Role of exergy in increasing efficiency and sustainability and reducing environmental impact," *Energy policy*, vol. 36, pp. 128-137, 2008.

[6] J. Szargut, *Exergy method: technical and ecological applications* vol. 18: WIT press, 2005.

[7] A. Yerrayya and P. Suresh, "Syngas Fueled Chemical Looping Combustion (Clc) Power Plant-Exergy Analysis," *Journal of Industrial Pollution Control*, vol. 32, 2016.

[8] A. Cihan, O. Hacıhafızog˘lu, and K. Kahveci, "Energy–exergy analysis and modernization suggestions for a combined-cycle power plant," *International Journal of Energy Research,* vol. 30, pp. 115-126, 2006.

[9] J. M. Montelongo-Luna, W. Y. Svrcek, and B. R. Young, "An exergy calculator tool for process simulation," *Asia-Pacific Journal of Chemical Engineering,* vol. 2, pp. 431-437, 2007.

[10] P. J. Baricelli, L. G. Melean, M. M. Alonso, A. Rodríguez, M. Rosales, and Á. González, "Advances in the aqueous-phase hydroformylation of olefins from a refinery naphtha cut: The effect of monoethanolamine in the catalytic activity of the Rh/TPPTS system," *Catalysis Today,* vol. 247, pp. 124-131, 2015.

[11] A. Wolff, "The Exergy Method of Thermal Plant Analysis. TJ KOTAS. Krieger, Florida, 1996, 328 Seiten, zahlr, Abb. u. Tab., brosch.,£ 35,–, ISBN 0-89464-946-9," *Chemie Ingenieur Technik*, vol. 69, pp. 1161-1161, 1997.

[12] M. Z. Stijepovic, A. Vojvodic-Ostojic, I. Milenkovic, and P. Linke, "Development of a kinetic model for catalytic reforming of naphtha and parameter estimation using industrial plant data," *Energy & Fuels*, vol. 23, pp. 979-983, 2009.

[13] A. Yong-an, G. Xing-quan, S. Lin, W. Yue-ren, and F. Guo-hui, "Exergy analysis of exhaust-gas of burning liquefied-gas in a Chinese kitchen," in *Energy and Environment Technology, 2009. ICEET'09. International Conference on*, 2009, pp. 40-43.

[14] M. Farmahini–Farahani, "Investigation of four geometrical parameters on thermal stratification of cold water tanks by exergy analysis," *International Journal of Exergy*, vol. 10, pp. 332-345, 2012.

[15] M. Boulenouar and A. Ouadha, "CFD-Exergy analysis of the flow in a supersonic steam ejector," in *Journal of Physics: Conference Series*, 2015, p. 012123.

[16] K. Alabi and F. Ladeinde, "Utilizing CFD-Based Exergy Calculations in the Design/Optimization of a Complete Aircraft System," in *45th AIAA Aerospace Sciences Meeting and Exhibit*, 2007, pp. 2007-1130.

[17] S. Jafarmadar, "Exergy analysis of natural gas/diesel combustion in homogenous charge compression ignition engines (HCCI) using multi-dimensional model," *International Journal of Exergy*, vol. 17, pp. 475-491, 2015.

[18] K. Taylor, A. G. Smith, S. Ross, and M. Smith, "The prediction of pressure drop and flow distribution in packed bed filters," in *Second International Conference on CFD in the Minerals and Process Industries, CSIRO*, 1999, pp. 273-280.

[19] R. Plascencia-Jatomea, F. Almazán-Ruiz, J. Gómez, E. Rivero, O. Monroy, and I. González, "Hydrodynamic study of a novel membrane aerated biofilm reactor (MABR): Tracer experiments and CFD simulation," *Chemical Engineering Science*, vol. 138, pp. 324-332, 2015.

[20] R. Mohammadikhah, S. Zahedi Abghari, M. Ahmadi-Marvast, and H. Ganji, "CFD simulation of catalytic naphtha reforming process," in *7th International Chemical Engineering Congress & Exihibition*, 2010, pp. 21-24.

[21] L. Shi, "Computational fluid dynamics simulation of steam reforming and autothermal reforming for fuel cell applications," Ohio University, 2009.

[22] E. Querol, B. Gonzalez-Regueral, and J. L. Perez-Benedito, *Practical approach to exergy and thermoeconomic analyses of industrial processes*: Springer Science & Business Media, 2012.

[23] J. M. Montelongo-Luna, W. Y. Svrcek, and B. R. Young, "The relative exergy array—a new measure for interactions in process design and control," *The Canadian Journal of Chemical Engineering,* vol. 89, pp. 545-549, 2011.

[24] M. Munir, W. Yu, and B. Young, "The relative exergy-destroyed array: A new tool for control structure design," *The Canadian Journal of Chemical Engineering,* vol. 91, pp. 1686-1694, 2013.

[25] A. M. Bahmanpour, A. Hoadley, and A. Tanksale, "Critical review and exergy analysis of formaldehyde production processes," *Reviews in Chemical Engineering,* vol. 30, pp. 583-604, 2014.

[26] X. Huang, J. Hong, Y. Zhang, Y. Shuai, Y. Yuan, B. Li, and H. Tan, "Exergy distribution characteristics of solar-thermal dissociation of NiFe 2 O 4 in a solar reactor," *Energy,* vol. 123, pp. 131-138, 2017.

[27] R. Mohammadikhah, S. Zahedi Abghari, H. Ganji, and M. Ahmadi Marvast, "Improvement of Hydrodynamics Performance of Naphtha Catalytic Reforming Reactors Using CFD," *Iranian Journal of Chemistry and Chemical Engineering (IJCCE),* vol. 33, pp. 63-76, 2014.

[28] D. Mehta and M. Hawley, "Wall effect in packed columns," *Industrial & Engineering Chemistry Process Design and Development,* vol. 8, pp. 280-282, 1969.

[29] S. Ergun, "Fluid flow through packed columns," *Chem. Eng. Prog.,* vol. 48, pp. 89-94, 1952.